

AD-A216 945

WRDC-TR-89-2067

ANALYTICAL AND EXPERIMENTAL INVESTIGATION OF
MINIATURE HEAT PIPES - PHASE II



G. P. Peterson and B. R. Babin
Mechanical Engineering Department
Texas A&M University
College Station, Texas 77843

24 June 1989

Final Report for Period March 88 - December 88

Approved for public release; distribution unlimited

DTIC
ELECTE
JAN 22 1990
S B D

AEROPROPULSION AND POWER LABORATORY
WRIGHT RESEARCH DEVELOPMENT CENTER
AIR FORCE SYSTEMS COMMAND
WRIGHT-PATTERSON AIR FORCE BASE, OHIO 45433-6563

90 01 22 0 41

NOTICE

When Government drawings, specifications, or other data are used for any purpose other than in connection with a definitely related Government procurement operation, the United States Government thereby incurs no responsibility nor any obligation whatsoever; and the fact that the government may have formulated, furnished, or in any way supplied the said drawings, specifications, or other data, is not to be regarded by implication or otherwise as in any manner licensing the holder or any other person or corporation, or conveying any rights or permission to manufacture use, or sell any patented invention that may in any way be related thereto.

This report has been reviewed by the Office of Public Affairs (ASD/PA) and is releasable to the National Technical Information Service (NTIS). At NTIS, it will be available to the general public, including foreign nations.

This technical report has been reviewed and is approved for publication.

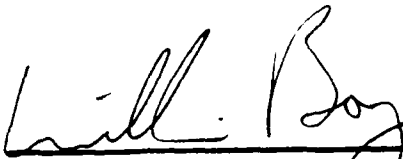


WON S. CHANG
Project Engineer



JERRY E. BEAM, TAM
Power Technology Branch
Aerospace Power Division
Aero Propulsion and Power Laboratory

FOR THE COMMANDER



WILLIAM U. BORGER
Chief, Aerospace Power Division
Aero Propulsion & Power Laboratory

If your address has changed, if you wish to be removed from our mailing list, or if the addressee is no longer employed by your organization please notify WRDC/POOS, W-PAFB, OH 45433 to help us maintain a current mailing list.

Copies of this report should not be returned unless return is required by security considerations, contractual obligations, or notice on a specific document.

UNCLASSIFIED

SECURITY CLASSIFICATION OF THIS PAGE

REPORT DOCUMENTATION PAGE

1. REPORT SECURITY CLASSIFICATION Unclassified			1b. RESTRICTIVE MARKINGS None		
2a. SECURITY CLASSIFICATION AUTHORITY			3. DISTRIBUTION / AVAILABILITY OF REPORT Approved for Public release; Distribution is unlimited		
2b. DECLASSIFICATION / DOWNGRADING SCHEDULE					
4. PERFORMING ORGANIZATION REPORT NUMBER(S)			5. MONITORING ORGANIZATION REPORT NUMBER(S) WRDC-TR-89-2067		
6a. NAME OF PERFORMING ORGANIZATION Texas A&M University		6b. OFFICE SYMBOL (If applicable)		7a. NAME OF MONITORING ORGANIZATION Aero Propulsion and Power Laboratory (WRDC/POOS) Wright Research Development Center	
6c. ADDRESS (City, State, and ZIP Code) Mechanical Engineering Department College Station, Texas 77843-3123			7b. ADDRESS (City, State, and ZIP Code) Wright-Patterson AFB, Ohio 45433-6563		
8a. NAME OF FUNDING / SPONSORING ORGANIZATION Aero Propulsion and Power Lab.		8b. OFFICE SYMBOL (If applicable) WRDC/POOS		9. PROCUREMENT INSTRUMENT IDENTIFICATION NUMBER F33615-86-C-2723	
8c. ADDRESS (City, State, and ZIP Code) Wright-Patterson AFB, Ohio 45433-6563			10. SOURCE OF FUNDING NUMBERS		
			PROGRAM ELEMENT NO. 63224C	PROJECT NO. L210	TASK NO. 00
			WORK UNIT ACCESSION NO. 26		
11. TITLE (Include Security Classification) "Analytical and Experimental Investigation of Miniature Heat Pipes - Phase II"					
12. PERSONAL AUTHOR(S) G. P. Peterson, D. Wu, B. Babin					
13a. TYPE OF REPORT Final		13b. TIME COVERED FROM 3/88 TO 12/88		14. DATE OF REPORT (Year, Month, Day) 1989 June 24	
15. PAGE COUNT 64					
16. SUPPLEMENTARY NOTATION					
17. COSATI CODES			18. SUBJECT TERMS (Continue on reverse if necessary and identify by block number)		
FIELD	GROUP	SUB-GROUP			
			Heat Pipe, Micro, Miniature, Modeling, Testing		
19. ABSTRACT (Continue on reverse if necessary and identify by block number) A combined experimental and analytical investigation was conducted in order to identify and better understand the phenomena which govern the performance limitations and operating characteristics of micro heat pipes - heat pipes so small that the mean curvature of the vapor-liquid interface is comparable in magnitude to the reciprocal of the hydraulic radius of the flow channel. The analytical portion of the investigation began by developing a steady-state model in which the effects of the extremely small characteristic dimensions on the conventional steady-state heat pipe modeling techniques were examined. To further understand the behavior of these types of devices, a transient analytical model was developed, which could be used to predict steady-state and transient behavior during start-up or variations in the evaporator thermal load. In the experimental portion of the investigation, two micro heat pipes, one copper and one silver, 1 mm in cross-sectional area and 57 mm in length, were evaluated experimentally to determine the accuracy of both the steady-state and transient model and to provide (continued on back)					
20. DISTRIBUTION / AVAILABILITY OF ABSTRACT <input checked="" type="checkbox"/> UNCLASSIFIED/UNLIMITED <input type="checkbox"/> SAME AS RPT. <input type="checkbox"/> DTIC USERS			21. ABSTRACT SECURITY CLASSIFICATION Unclassified		
22a. NAME OF RESPONSIBLE INDIVIDUAL W. S. Chang			22b. TELEPHONE (Include Area Code) (513) 255-6241		22c. OFFICE SYMBOL WRDC/POOS

9. Abstract (Continued)

verification of the micro heat pipe concept. Tests were conducted in a vacuum environment to eliminate conduction and convection losses.

The steady-state experimental results obtained were compared with the analytical model and verified the modeling predictions for both the steady-state model and the transient model (at steady-state). The steady-state model overpredicted the experimentally determined maximum heat transport capacity by approximately 30 percent for both the copper and silver test pipes. The transient model (at steady-state), however, proved to be significantly more accurate with the difference between the measured and predicted values averaging less than 10 percent for the copper test pipe and 5 percent for the silver test pipe.

In addition to accurately predicting the maximum heat transport capacity, the results indicated that reverse liquid flow occurs in the liquid channels during start-up and the wetting angle is the single most important factor contributing to the transport capacity and behavior of these micro heat pipes.

TABLE OF CONTENTS

I.	INTRODUCTION	1
	1.1 Background	1
	1.2 Research Objectives	2
II.	STEADY-STATE MODEL	3
	2.1 The Capillary Limitation	5
	2.1.1 Conventional Method	6
	2.1.2 Cotter's Method	12
	2.2 The Viscous Limitation	15
	2.3 The Sonic Limitation	15
	2.4 The Entrainment Limitation	16
	2.5 The Boiling Limitation	17
	2.6 Discussion of Steady-State Modeling Results	17
III.	TRANSIENT MODEL	25
	3.1 Modeling Assumptions	25
	3.2 Governing Equations	26
	3.3 Modeling Approach	29
	3.3.1 Evaporator Region	29
	3.3.2 Adiabatic Region	30
	3.3.3 Condenser Region	30
	3.4 General Assembly	31
	3.5 Discussion of Transient Modeling Results	32
	3.5.1 Geometry	32
IV.	EXPERIMENTAL PROGRAM	46
	4.1 Description of Test Article	46
	4.2 Description of Experimental Apparatus	46
	4.3 Experimental Procedure	50
V.	RESULTS AND CONCLUSIONS	51
	5.1 Comparison of Analytical and Experimental Results	55
	5.2 Summary	60
VI.	NOMENCLATURE	63
	REFERENCES	65



Accession For	
NTIS GRA&I	<input checked="" type="checkbox"/>
DTIC TAB	<input type="checkbox"/>
Unannounced	<input type="checkbox"/>
Justification	
By _____	
Distribution/	
Availability Codes	
Dist	Avail and/or Special
A-1	

I. INTRODUCTION

1.1 Background

The need to develop microelectronic devices capable of operating at increased performance levels with high reliability, requires better methods of thermal control. With the recent trend towards increased miniaturization and component density, the thermal management problem increases dramatically. This is particularly true in the microelectronic components proposed for use in spacecraft applications where the heat removal capacity of the thermal control systems governs the physical size of both the individual components and overall systems.

In 1984, Cotter described very small, micro heat pipes for cooling microelectronic devices. He defined a micro heat pipe as "one so small that the mean curvature of the vapor-liquid interface is necessarily comparable in magnitude to the reciprocal of the hydraulic radius of the total flow channel." Mathematically, this can be expressed as

$$r_c \propto \frac{1}{r_h} \quad (1)$$

where r_c is the mean curvature of the vapor-liquid interface and r_h is the hydraulic radius of the total flow channel. This relationship can be better defined by nondimensionalizing both the mean curvature of the vapor-liquid interface and the hydraulic radius, i.e., dividing both by r_c , prior to substitution into equation 1. This yields an expression which more precisely defines a micro heat pipe as one which satisfies the condition that

$$\frac{r_c}{r_h} \geq 1 \quad (2)$$

In practical terms, a micro heat pipe is a wickless, noncircular channel with an approximate diameter of 100 to 1000 μm and a length of about 10 to 20 mm. Unlike traditional heat pipes, micro heat pipes would not have a wick but would use the mean curvature of the channel to pump the liquid from the condenser to the evaporator, which would be an integral part of the device. Besides the difficulties of manufacturing, cleaning, and filling these miniature heat pipes, they would be very sensitive to the amount of working fluid present. Since the liquid-vapor interface changes continually along the pipe, care must be taken to ensure proper wetted conditions without flooding. These unique devices may play an important role in future microelectronic devices where thermal loads are high and space is at a premium.

1.2 Research Objectives

To identify and better understand the phenomena which govern the performance limitations and operating characteristics of micro heat pipes, a combined experimental and analytical investigation was conducted. The objectives of this investigation were twofold:

- i. Develop an analytical model capable of predicting the steady-state operational characteristics and performance limitations of a micro heat pipe.
- ii. Obtain and test several micro heat pipes to determine the effects of the amount of working fluid, the shape of the capillary wicking structure, the operating temperature, the evaporator heat flux, and the effects of gravity on the heat transport capacity and performance limitations.

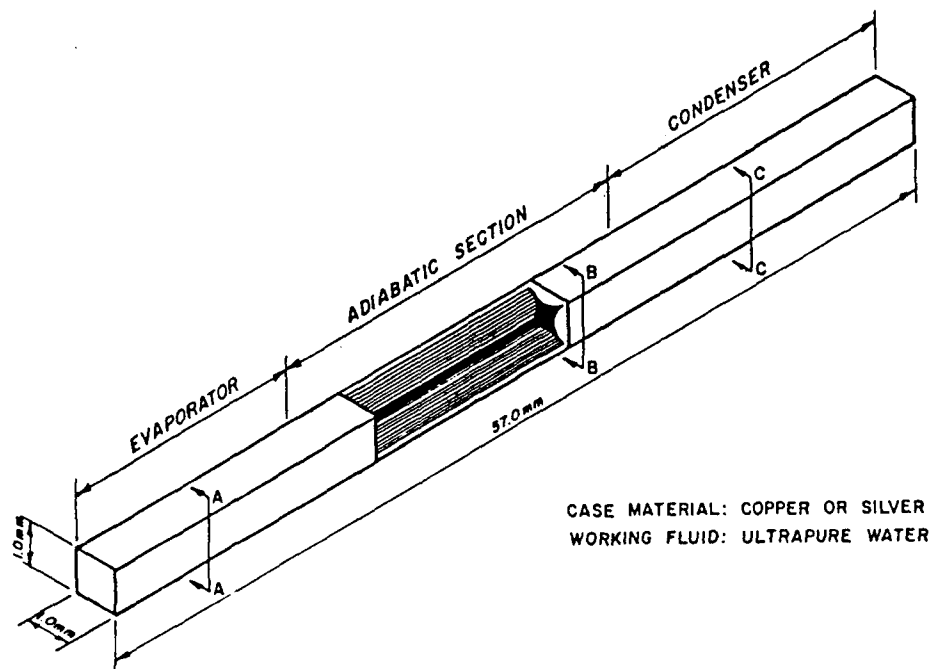
Presented here is a description of a steady-state analytical model and the methodology utilized in the development of that model along with a description of the experimental portion of the investigation, including a description of the test article, the experimental apparatus, and the experimental procedure followed. In Section IV, the experimental results are compared with the

predicted results obtained from the steady-state analytical model.

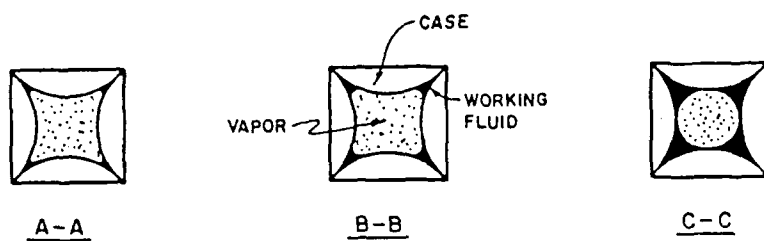
Figure 1 illustrates the general shape of the heat pipe being modeled, along with the liquid configuration, and Fig. 2 illustrates the critical cross-sectional dimensions. As shown, the outer dimensions are 1 mm by 1 mm and the length is 57 mm. The case material is either copper or silver and the working fluid is water. This heat pipe is considerably smaller than most heat pipes and because of this, the triangular grooves in the corners of the heat pipe can serve as arteries for the return of liquid (i.e., the wicking structure). Because of the size of the heat pipe tested, it was very difficult to measure the thermal-hydraulic parameters within the pipe during operation. For this reason, in addition to accomplishing the two objectives outlined above, a transient analytical model was developed for the micro heat pipe. This model is capable of predicting the transient behavior during start-up or during variations in the thermal load in the evaporator portion of the heat pipe. Using this model, the time required to reach steady-state can be predicted along with the effect of variations in the amount and type of fluid and the cross-sectional shape. A detailed description of the methodology used in the development of this transient model along with a comparison of the steady-state experimental results and the steady-state results obtained from the transient model are presented.

II. STEADY-STATE MODEL

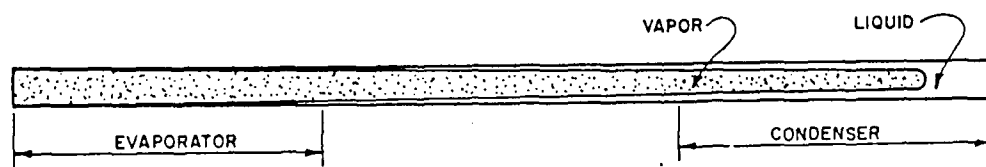
Although the fundamental phenomena involved in the operation of micro heat pipes may be different from those occurring in larger heat pipes, traditional steady-state modeling techniques can be used as a first estimate of the operational characteristics and performance limitations. Following is a discussion of the traditional limitations of heat pipes and how they pertain to the configuration described above.



MICRO HEAT PIPE



SECTIONS



AXIAL LIQUID DISTRIBUTION

Fig. 1 Trapezoidal micro heat pipe.

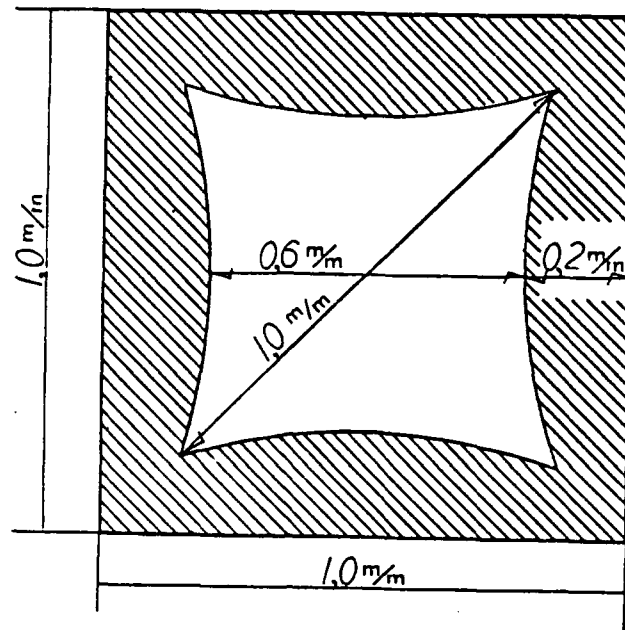


Fig. 2 Cross-sectional shape and dimensions of the trapezoidal micro heat pipe.

2.1 The Capillary Limitation

Because of the size and wicking structure of micro heat pipes, we anticipated that they will be limited by capillary forces. The operation of a heat pipe requires the capillary pumping pressure to be greater than all other resisting pressures; the hydrostatic pressure, the liquid pressure, and the vapor pressure. The governing relation is expressed by the equation

$$\Delta P_c \geq \Delta P_{||} + \Delta P_l + \Delta P_v \quad (3)$$

The capillary pumping pressure (ΔP_c) is the pressure difference between the evaporator and condenser ends of the heat pipe at the liquid and vapor interface. The hydrostatic pressure drop ($\Delta P_{||}$) is due to the body forces. The

vapor (ΔP_v) and liquid (ΔP_l) pressure drops are due to viscous forces in the vapor and liquid, respectively.

Two methods will be discussed, both of which describe how this limit can be used to predict steady-state operation. The first method is an adapted version of conventional heat pipe theory while the second method has been specifically developed for micro heat pipes.

2.1.1. The Conventional Method. The conventional method involves defining each of the pressure terms in equation (1) independently and then combining them to solve for the maximum heat flux.

First, it is necessary to develop a relationship for the capillary pumping pressure. Reducing the LaPlace-Young equation results in

$$\Delta P_c = \frac{2\sigma}{r_{ce}} - \frac{2\sigma}{r_{cc}} \quad (4)$$

where r_{ce} and r_{cc} are the radii of curvature of the fluid at the evaporator and condenser regions, respectively and σ is the surface tension of the fluid. Because of vaporization at the evaporator region of the heat pipe, the liquid meniscus recedes in the triangular groove. Also, in the condenser section condensation causes the liquid meniscus to be flooded. This resulting difference in radii of curvature causes a pressure difference and hence, pumping of the liquid from the condenser to the evaporator. It is generally assumed that r_{cc} approaches infinity during steady-state operation which allows the capillary pressure to be only a function of the evaporator capillary radius, or

$$\Delta P_c = (2\sigma/r_{ce}) \quad (5)$$

The wicking structure used in micro heat pipes can be approximated as triangular grooves. Chi (1976) found that for triangular grooves

$$r_{ce} = w/\cos(a) \quad (6)$$

where w is the groove width and a is the half-included angle.

The axial hydrostatic pressure drop is a result of the body forces acting along the longitudinal axis. This is expressed as

$$\Delta P_{||} = \rho_l g L_p \sin(\phi) \quad (7)$$

where L_p is the overall length of the heat pipe and ϕ is the angle the heat pipe makes with respect to the horizontal.

The third term necessary is the liquid pressure drop. The viscous forces in the liquid result in a pressure drop which resists the capillary flow through the wick. Since the liquid pressure gradient may vary along the longitudinal axis of the heat pipe, the total liquid pressure drop can be determined by integrating the pressure gradient over the length of the flow passage, or

$$\Delta P_l(z) = - \int_0^z \frac{dP_l}{dz} dz \quad (8)$$

where the limits of integration are from the evaporator end to the condenser end ($z=0$) and dP_l/dz is the gradient of the liquid pressure resulting from frictional drag. This frictional drag, due to the shear stress, can be written as

$$\frac{dp_l}{dz} = - \frac{2\tau_l}{(r_{h,l})} \quad (9)$$

where τ_l is the frictional shear stress at the liquid-solid interface and $r_{h,l}$ is the hydraulic radius, defined as twice the cross-sectional area

divided by the wetted perimeter.

At this point, the Reynolds number, Re_1 , and drag coefficient, f_1 , can be introduced as

$$Re_1 = \frac{2(r_{h,1})\rho_1 V_1}{\mu_1} \quad (10)$$

and

$$f_1 = \frac{2\tau_1}{\rho_1 V_1^2} \quad (11)$$

where V_1 is the local liquid velocity which is related to the local heat flow by the equation

$$V_1 = \frac{Q}{\epsilon A_g \rho_1 L} \quad (12)$$

In this expression, A_g is the groove cross-sectional area, ϵ is the wick porosity, and L is the latent heat of vaporization.

Combining equations (8) through (10) with (7) yields,

$$\frac{dp_1}{dz} = - \left(\frac{(f_1 Re_1) \mu_1}{2 \epsilon A_g (r_{h,1})^2 L \rho_1} \right) Q \quad (13)$$

This equation can be written as

$$\frac{dp_1}{dz} = - \left(\frac{\mu_1}{K A_g L \rho_1} \right) \quad (14)$$

where K is the permeability expressed as

$$K = \frac{2 \epsilon (r_{h,1})^2}{(f_1 Re_1)} \quad (15)$$

For laminar flow, $(f_1 Re_1)$ is constant and depends only on the passage shape. Thus, the permeability, K , is independent of the flow path. For triangular grooves

$$K = \frac{(d_h)^2}{4B} \quad (16)$$

where d_h is the hydraulic diameter and B is a constant with a value of 30 for smooth copper or silver.

For the axial direction with constant heat addition and removal, equation (12) can be substituted into equation (6) and integrated over the length of the heat pipe to yield

$$\Delta P_1 = \left(\frac{\mu_1}{KA_g L \rho_1} \right) L_{eff} Q_c \quad (17)$$

where L_{eff} is the effective heat pipe length defined as

$$L_{eff} = 0.5L_e + L_a + 0.5L_c \quad (18)$$

Determination of the vapor pressure drop in heat pipes is complicated by the mass addition and removal in the evaporator and condenser respectively, and by the compressibility of the vapor phase. Performing a mass balance on a section of the adiabatic region of the heat pipe ensures that for continued operation, the liquid mass flow rate and vapor mass flow rate must be equal. Because of the large difference in the density of these two phases, the velocity of the vapor phase must necessarily be significantly higher than the velocity of the liquid phase. For this reason, in addition to the pressure gradient resulting from frictional drag, the pressure gradient due to variations in the dynamic pressure must also be considered. Both Chi (1976) and Dunn and Reay (1983) have addressed this problem. Chi (1976) found that upon integration of the

vapor pressure gradient, the dynamic pressure effects cancel. The result is an expression, which is similar to that developed for the liquid,

$$\Delta P_v = \left(\frac{C(f_v Re_v) \mu_v}{2(r_{h,v})^2 A_v \rho_v L} \right) L_{eff} Q_c \quad (19)$$

where $r_{h,v}$ is the hydraulic radius of the vapor space and C is a constant, which depends on the Mach Number.

As mentioned previously, during steady-state operation, at any axial position, the liquid mass flow rate, \dot{m}_l , must equal the vapor mass flow rate, \dot{m}_v , and while the liquid flow regime is always laminar, the vapor flow may be either laminar or turbulent. It is therefore necessary to determine the vapor flow regime as a function of the heat flux. This can be accomplished by evaluating the local axial Reynolds number in the vapor, defined as

$$Re_v = \frac{2r_{h,v} Q}{A_v \mu_v L} \quad (20)$$

In addition, it is necessary to determine if the flow should be treated as compressible or incompressible by evaluating the local Mach number, defined as

$$Ma_v = \frac{Q}{A_v \rho_v L (R_v T_v \gamma)^{.5}} \quad (21)$$

where R_v is the gas constant, T_v is the vapor temperature and γ is the ratio of specific heats, which is equal to 1.67, 1.4, or 1.33 for monatomic, diatomic, and polyatomic vapor, respectively (Chi, 1976).

Previous investigations summarized by Kraus and Bar-Cohen (1983) have demonstrated that the following combinations of these conditions can be

used with reasonable accuracy.

$$Re_v \leq 2300, Ma_v \leq 0.2 \quad (22)$$

$$(f_v Re_v) = 16$$

$$C = 1.00$$

$$Re_v \leq 2300, Ma_v < 0.2 \quad (23)$$

$$(f_v Re_v) = 16$$

$$C = C_1 = \left[1 + \left(\frac{\gamma - 1}{2} \right) Ma_v^2 \right]^{0.5}$$

$$Re_v > 2300, Ma_v \leq 0.2 \quad (24)$$

$$(f_v Re_v) = 0.038$$

$$C = C_2 = \left(\frac{2r_{h,v} Q}{A_v L \mu_v} \right)^{\frac{3}{4}}$$

$$Re_v > 2300, Ma_v > 0.2 \quad (25)$$

$$(f_v Re_v) = 0.038$$

$$C = C_1 C_2$$

Since the equations used to evaluate both the Reynolds number and the Mach number are functions of the heat transport capacity, it is necessary to first assume the conditions of the vapor flow. Using these assumptions, the maximum heat capacity, $Q_{c,m}$, can be determined by substituting the values of the individual pressure drops into equation (1) and solving for $Q_{c,m}$. The overall solution for the heat transport capacity as limited by the capillary forces of the wicking structure is then

$$Q_{c,m} = \frac{\frac{2\sigma}{r_{ce}} - \rho_l g L \sin(u)}{L_{eff} \left(\frac{\mu_l}{KA_g L \rho_l} + \frac{C(f_v Re_v) \mu_v}{2(r_{h,v})^2 A_v \rho_v L} \right)} \quad (26)$$

with the values for C and $f_v Re_v$ found iteratively, depending on the vapor flow regime.

2.1.2. Cotter's Method. Cotter (1984) developed a steady-state equation that described the capillary limit specifically for micro heat pipes. Since this method applies only to micro heat pipes many simplifying assumptions were made. These assumptions will be discussed as the final equation is developed.

This development begins with restating equation (1). By summing the pressures throughout the fluid flow passage, an expression for the liquid-vapor pressure difference can be obtained

$$P_v - P_l = \frac{\sigma}{r_m} \quad (27)$$

where P_v and P_l are the vapor and liquid pressures and r_m is the mean radius of curvature given by

$$\frac{1}{r_m} = \frac{1}{r_{cc}} + \frac{1}{r_{ce}} \quad (28)$$

Simplifying the momentum equation, the equation of the fluid in steady-state parallel flow becomes

$$\mu \left(\frac{\delta^2 w}{\delta x^2} + \frac{\delta^2 w}{\delta y^2} \right) = \frac{dP}{dz} \quad (29)$$

where w is the axial fluid velocity. For a uniform cross-sectional area, A , having $w=0$ on the boundaries, we can transform to new dimensionless

variables x' , y' , and w' given by

$$x = A^{1/2} x'; y = A^{1/2} y'; w = -\frac{A}{\mu} \frac{dP}{dz} w' \quad (30)$$

Substituting these variables into equation (29) satisfies

$$\frac{\delta w'}{\delta x'^2} + \frac{\delta w'}{\delta y'^2} = -1 \quad (31)$$

Again substituting the dimensionless variables into the local mass flow equation,

$$m = \rho \iint w dx dy \quad (32)$$

the result is

$$m = -\frac{K' \rho A^2}{8 \mu} \frac{dP}{dz} \quad (33)$$

where K' is a shape factor given by

$$K' = 8 \pi \iint w' dx' dy' \quad (34)$$

Values for K' have been developed by Cotter (1984) and are presented in Table 1.

Table 1
Flow Shape Factor Values

Shape	K'
Circle	1.000
Regular Hexagon	0.964
Square	0.883
Triangle, 60-60-60	0.725
Triangle, 45-55-90	0.656
Triangle, 30-60-90	0.597

Solving for the pressure differential in both the vapor and liquid cases and substituting this into equation (27) yields

$$\frac{8\pi v_v^m}{K'_v A_v^2} = \frac{8\pi v_l^m}{K'_l A_l^2} - \frac{d}{dz} \frac{\sigma}{R} \quad (35)$$

Realizing that for steady-state, the local liquid and vapor mass flow rates are equal in magnitude and proportional to the local heat flux, Q , the mass flow rate can be calculated as

$$\dot{m}_v(z) = -\dot{m}_l(z) = \frac{Q}{L} h(z/L_p) \quad (36)$$

and the total area can be given by

$$A(z) = A_l(z) + A_v(z) \quad (37)$$

At this point, it is convenient to relate A_l and R with a geometrically determined dimensionless variable, β , by the equation

$$A_l = \beta^2 R^2 \quad (38)$$

Now by substituting equations (36) through (38) into equation (35) and solving, a first order ordinary differential equation is obtained which relates the radius of curvature to the axial position along the pipe, or

$$\frac{dR}{dz} = \frac{8\pi Q r_m h(z/L_p)}{\sigma L} \left(\frac{v_v}{K'_v (A - \beta^2 r_m^2)^2} + \frac{v_l}{K'_l \beta^4 r_m^4} \right) \quad (39)$$

Since the cross-sectional area, A , is assumed a constant, this equation is separable and therefore solvable. The solution is

$$Q_{\max} = \left(\frac{0.16\beta(K'_l K'_v)^{1/2}}{8\pi h(L_p)} \right) \left(\frac{\sigma L}{v_l} \right) \left(\frac{v_l}{v_v} \right)^{1/2} \left(\frac{A^{3/2}}{L_p} \right) \quad (40)$$

where H is the integral of h over the length of the pipe, as presented by Cotter (1984).

2.2 Viscous Limitation

Vapor flow to the condenser relies on the pressure difference between the condenser and evaporator. At low temperatures, the pressure difference across the heat pipe is not great enough to overcome the viscous forces that exist at these conditions. Dunn and Reay (1983) found this limitation, called the viscous limit, to be evaluated by the equation

$$q_v = \frac{r_v^2 L \rho_v P_v}{16 \mu_v L_{eff}} A_v \quad (41)$$

where P_v is the vapor pressure within the heat pipe. For most cases this limit may be neglected.

2.3 The Sonic Limitation

Sonic limitations in heat pipes are analogous to the sonic limitations in converging-diverging nozzles (Chi, 1976). In a converging-diverging nozzle, the mass flow rate is constant and the vapor velocity varies because of the changing cross-sectional area. In heat pipes, the reverse occurs; the area is constant and the vapor velocity varies because of the evaporation and condensation along the heat pipe. As in nozzle flow, decreased outlet pressure, or in this case condenser temperature, results in a decrease in the evaporator temperature until the sonic limitation is reached. Any further increase in the heat rejection rate does not reduce the evaporator temperature or the maximum heat transfer capability, but only reduces the condenser temperature, because of the existence of choked flow.

The sonic limitation in heat pipes can be determined as

$$q_s = A_v P_v L \left(\frac{\gamma R_v T_v}{2(\gamma + 1)} \right)^{1/2} \quad (42)$$

where T_v is the mean vapor temperature within the heat pipe.

2.4 The Entrainment Limitation

Since the liquid and vapor flow in opposite directions in a heat pipe, at high enough vapor velocities, liquid droplets may be picked up or entrained in the vapor flow. This entrainment results in excess liquid accumulation in the condenser and hence, dryout of the wicking structure. Therefore, it is necessary to evaluate when the onset of entrainment begins in a counter-current, two-phase flow. The most commonly quoted criterion to determine this onset is when the Weber number, We , defined as the ratio of the viscous shear force to the force resulting from the liquid surface tension or

$$We = \frac{2(r_{h,g}) \rho_v V_v^2}{\sigma} \quad (43)$$

is equal to unity. To prevent the entrainment of liquid droplets in the vapor flow, the Weber number must therefore be less than one.

By relating the vapor velocity to the heat transport capacity

$$V_v = \frac{Q}{A_v \rho_v L} \quad (44)$$

a value for the maximum transport capacity based on the entrainment limitations may be determined as

$$q_e = A_v L \left(\frac{\sigma \rho_v}{2r_{h,g}} \right)^{1/2} \quad (45)$$

where $r_{h,g}$ is the hydraulic radius of the groove. A somewhat different

approach has been proposed by Rice and Fulford (1987) who developed an expression that defines the critical dimensions for wicking structures in order to prevent entrainment.

2.5 The Boiling Limitation

When sufficient heat is applied to the evaporator of a heat pipe, boiling may occur and hence trap bubbles in the wick. This trapping of bubbles blocks the return of fluid to the evaporator and causes dryout of the wick, a phenomenon referred to as the boiling limit. The actual formulation of this limit is based on nucleate boiling theory. For a heat pipe with an axial evaporator, this limit is described by the equation

$$q_b = \frac{2\pi L_e k_e T_v}{L \rho_v \ln(r_i/r_v)} \left(\frac{2\sigma}{r_n} - \Delta P_{c,m} \right) \quad (46)$$

where k_e is the effective conductivity, r_i is the inner radius of the heat pipe, r_v is the vapor core radius and r_n is the nucleation radius. Investigations by Chi (1976) have found the nucleation radius to be within a range of 2.54×10^{-5} to 2.54×10^{-7} meters for conventional heat pipes.

2.6 Discussion of the Steady-State Modeling Results

To compare the previously described limitations, a FORTRAN computer code was developed. This computer file calculates all the limits previously mentioned except the boiling limit. The limits can be calculated as a function of the operating temperature or tilt angle. The working fluid can be selected from four working fluids, water, methanol, ammonia, or acetone.

The input dimensions used in the calculation of the limits presented in the following discussion are listed in Table 2. The calculation of Cotter's capillary limit required the several dimensionless constants obtained from the original paper. These values are presented in Table 3 for clarity. It is

significant to note that since one of the assumptions was that the heat pipes had been properly charged, the performance is not affected by the amount of working fluid present.

Table 2 Micro Heat Pipe Dimensions

length	0.05 m
condensor length	0.0127 m
evaporator length	0.0127 m
w	0.000133 m
a	0.5854 rad
vapor channel diameter	0.0006 m

Table 3 Dimensionless Constants

$H(L_p)$	0.5
K'_l	0.600
K'_v	0.975
B	2.044

As illustrated in Fig. 3, the capillary limit is clearly the controlling limit for micro heat pipe operation, since both the conventional method and Cotter's method of calculation of the capillary limit are well below the other limits. For this reason, further discussion will focus on the capillary limit only.

The development of the two methods used to calculate the capillary limit have some significant differences. A few basic assumptions are shared between the two methods. These are:

- the heat pipe is properly charged
- the length to diameter ratio is much greater than one
- the cross-sectional area is relatively constant
- the vapor and liquid are at the same constant temperature

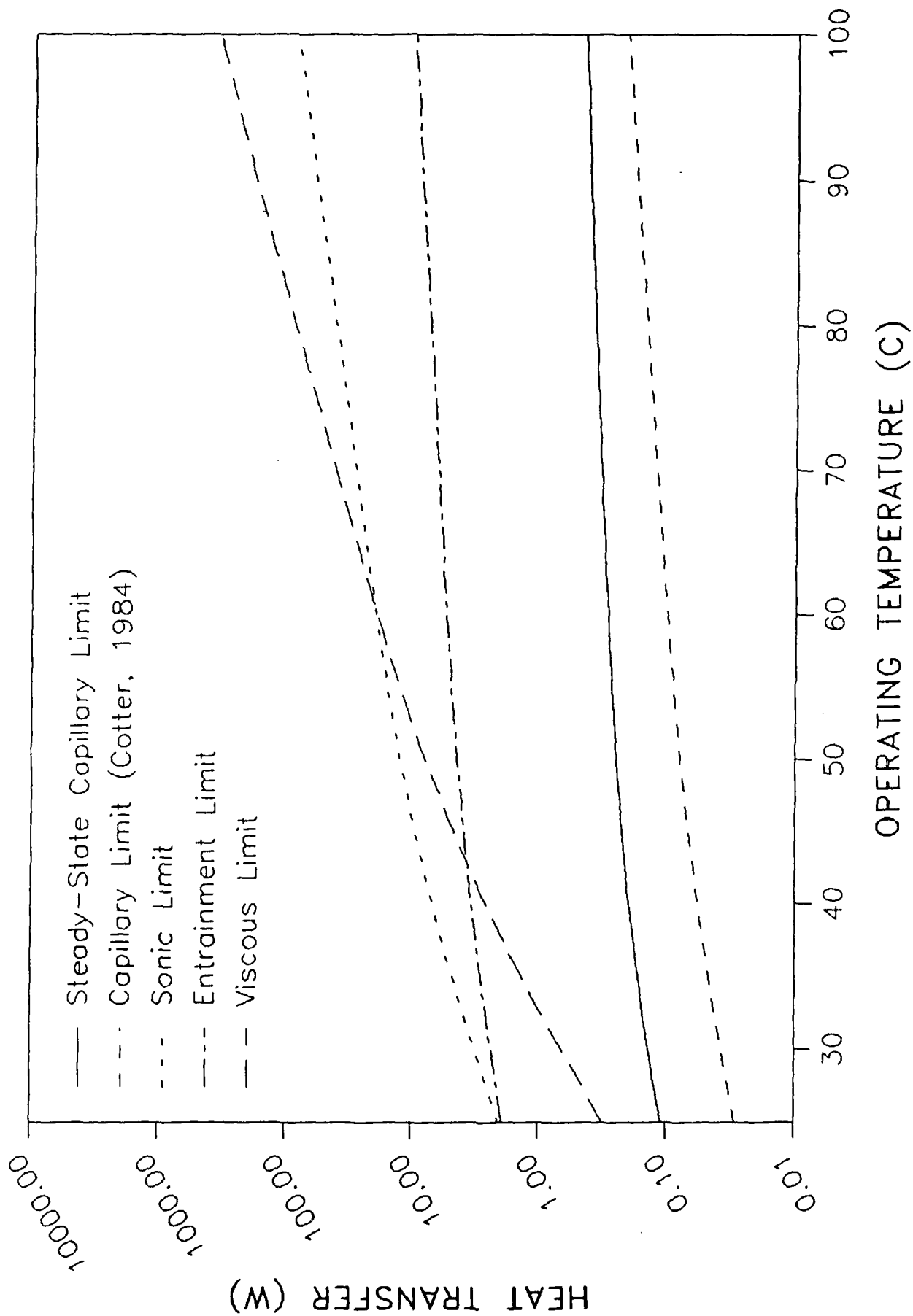


Fig. 3 Limitations of the trapezoidal micro heat pipe with water at a horizontal orientation.

The steady-state model described earlier, makes no further assumptions while the method proposed by Cotter (1984), assumes:

- gravity is negligible
- the local axial heat transfer is specified
- the liquid-vapor interface velocity is zero
- the vapor flow regime is both laminar and incompressible

To determine the significance of the gravitational forces, Figs. 4, 5, and 6 are provided. For the case of a horizontal heat pipe with water as the working fluid, Fig. 4, the gravitational effects which appear in the hydrostatic pressure term as the horizontal axis are clearly negligible. However, when the temperature is held constant and the tilt angle is varied, Fig. 5, the gravitational effects become more apparent. Figure 6 illustrates how the performance of a micro heat pipe as predicted by steady-state model diminishes when the wicking structure has to work against gravity. Together, Figs. 5 and 6 illustrate that as is the case for conventional heat pipes, for increasing tilt, the heat transport of the heat pipe decreases. This would indicate that at a tilt angle other than zero (horizontal), gravity has a significant effect on the capillary limit and cannot be assumed negligible.

The assumption that the local axial heat transport be specified, results in a parameter, $H(L)$, which must be known a priori to predict the maximum transport capacity. In this sense, it behaves as a correction factor which can be varied to better simulate the experimental results, but is of little value in actually predicting the performance limitation prior to testing. Figure 7 illustrates the effect of this parameter on the capillary limit as predicted by Cotter (1984). As shown, variation of this parameter results in significant variations in the predicted transport capacity with a value of 0.25 resulting in the closest correlation between the two techniques.

Two additional assumptions were made in the development of the Cotter

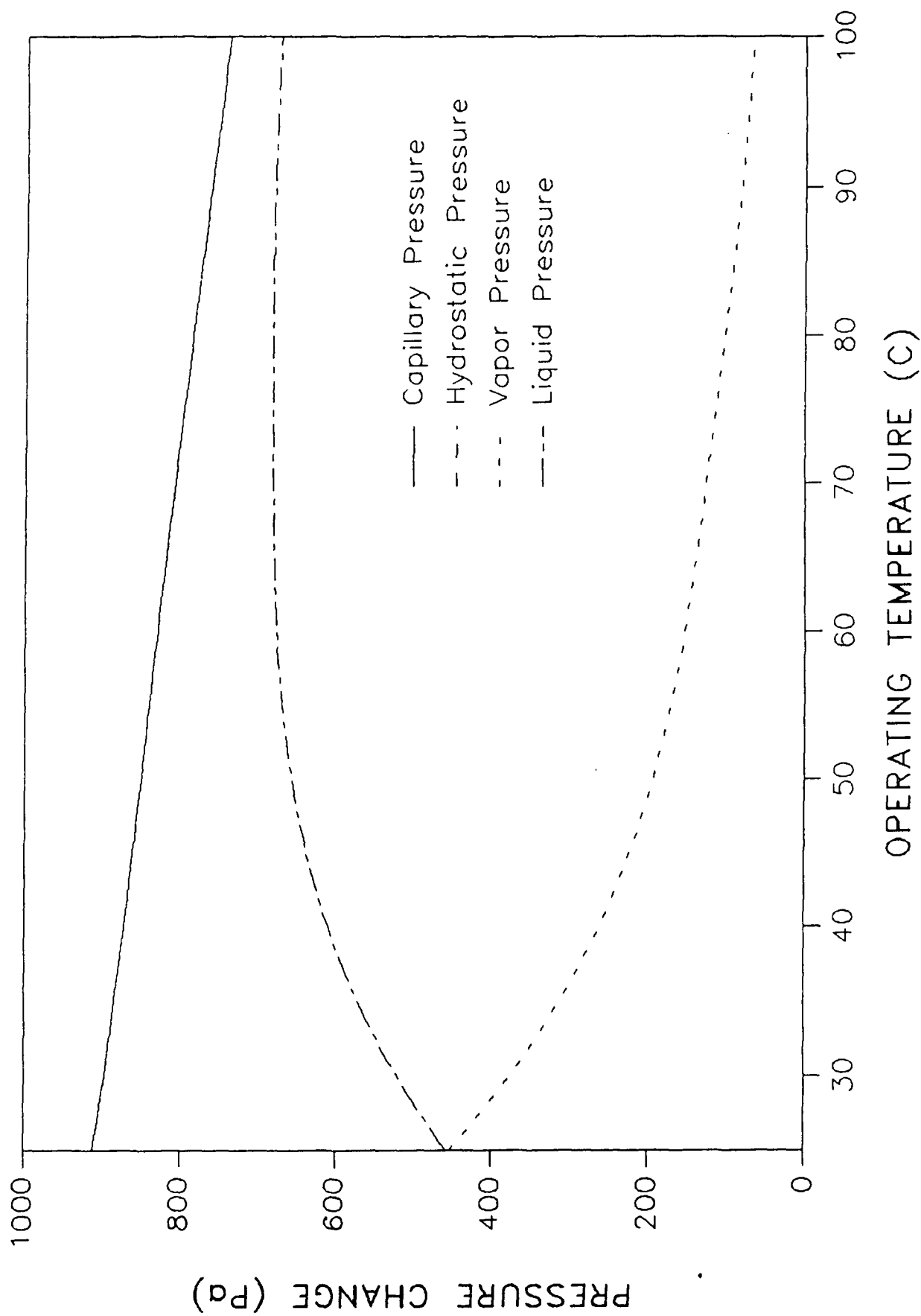


Fig. 4 Evaluation of the pressure components as a function of the tilt angle for the trapezoidal heat pipe with water at 25°C.

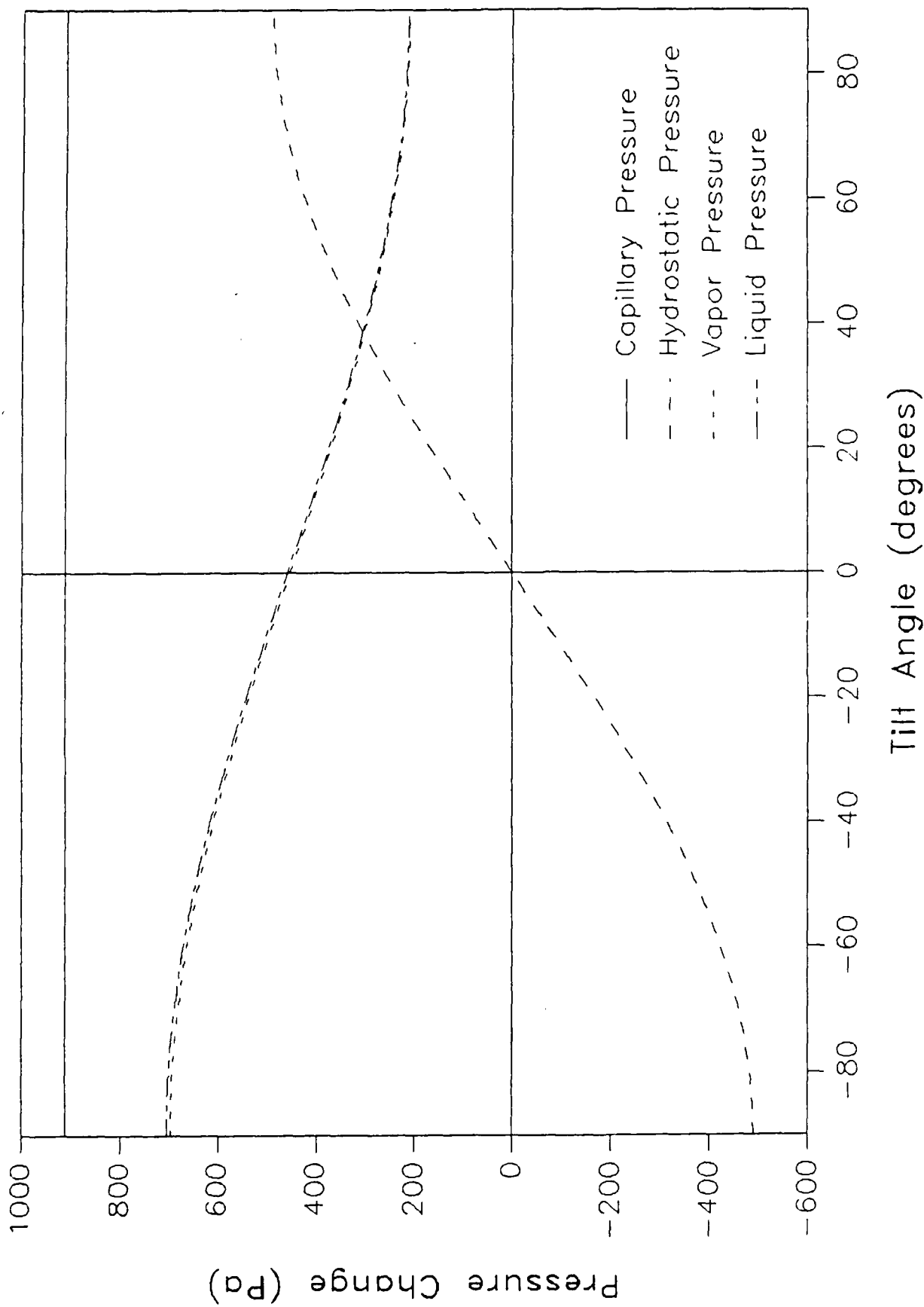


Fig. 5 Evaluation of the pressure components as a function of the operating temperature for the trapezoidal heat pipe with water at a horizontal orientation.

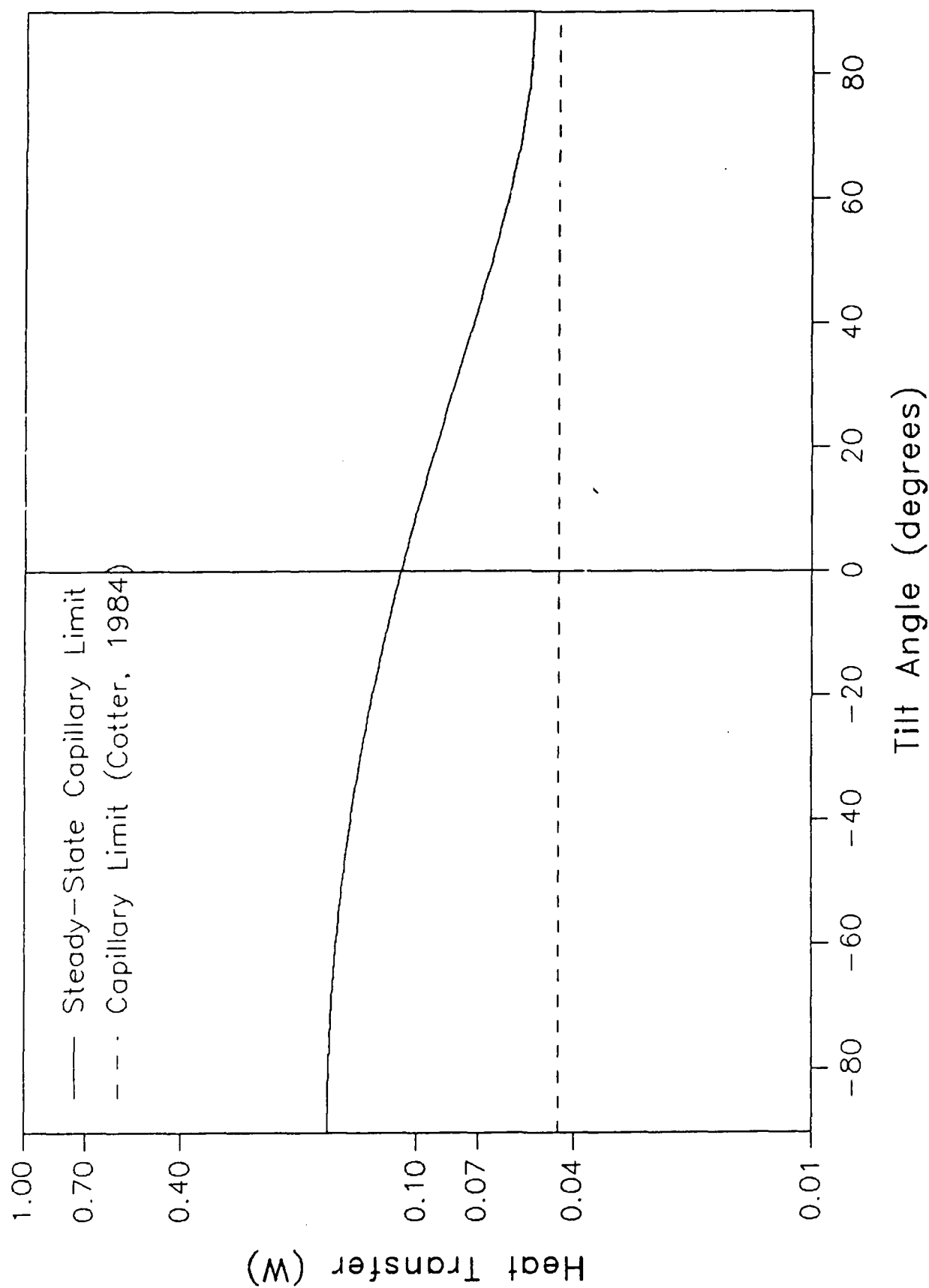


Fig. 6 Comparison of the capillary limits as a function of the tilt angle for the trapezoidal heat pipe with water at 25°C.

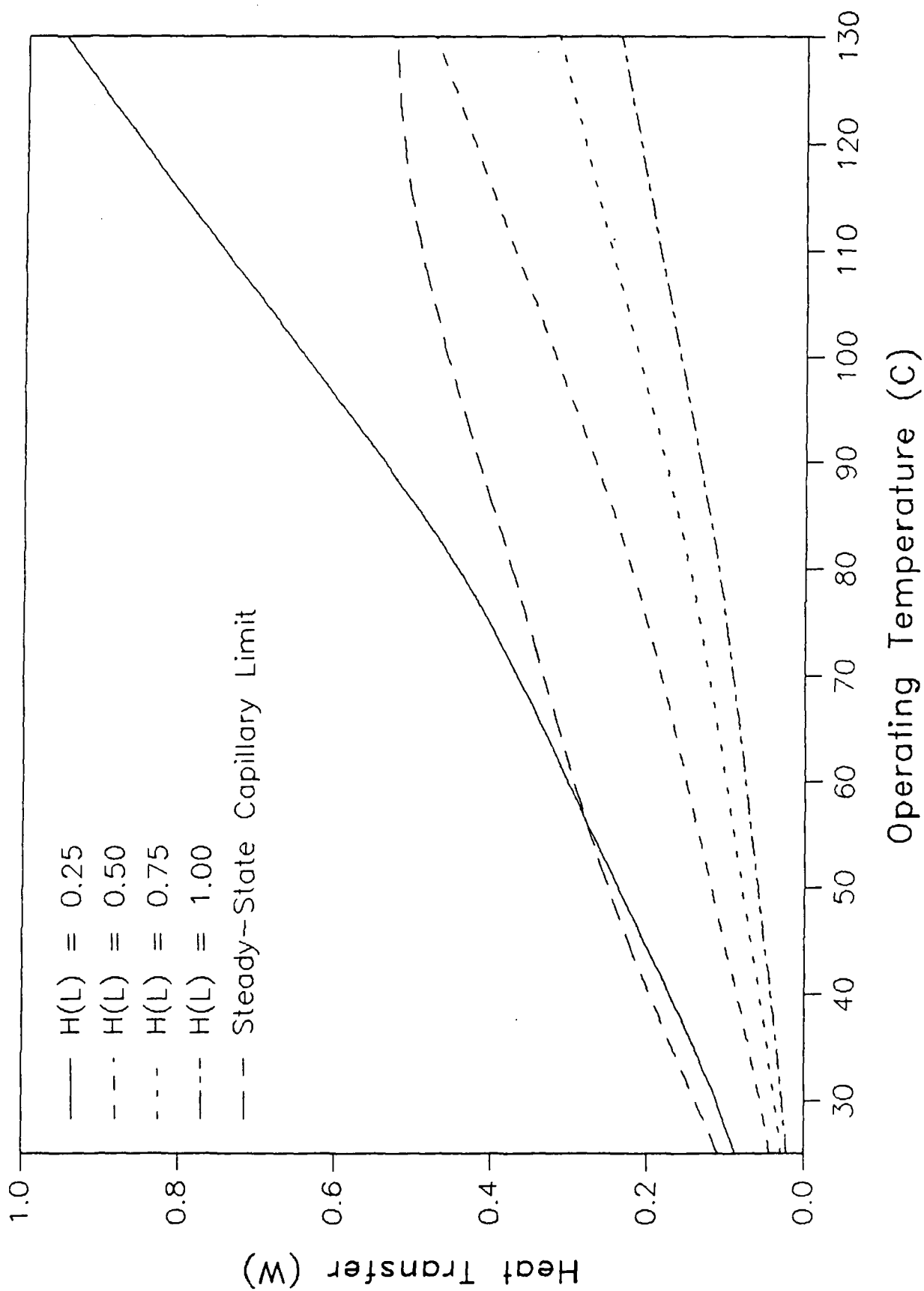


Fig. 7 Effect of variations in the local axial heat flux model (Cotter, 1984) on the maximum heat transport capacity.

model. First, is that the liquid-vapor interface velocity is zero. Although this introduces some error, it is small and is necessary in order to proceed. Second, is the assumption that the vapor flow regime is both laminar and incompressible. In all of the cases evaluated, the flow regime of the vapor was found to be in a region that would make this assumption both reasonable and appropriate.

III. TRANSIENT MODEL

To understand the effects of parameters such as the geometry, the liquid-solid contact angle, and the amount of working fluid, knowledge of the transient behavior is required. This coupled with the small size, it is very difficult to measure the thermal-hydraulic parameters within a given pipe during operation resulted in the development of a transient model capable of predicting the behavior during start-up or during variations in the thermal load in the evaporator portion of the heat pipe. The steady-state modeling predictions made previously indicate that the boiling, sonic, and entrainment limits for heat pipes of this geometry are well above the capillary limits and as a result, the model considers only the capillary limit. Also, because of the symmetry of the heat pipe, a one-dimensional model was used with all of the variables presented as functions of x , the position along the heat pipe, and/or t , the amount of time since the last change in the evaporator power level.

3.1 Modeling Assumptions

To better understand the capability and limitations of the transient model, the following is a list of the assumptions made. We attempted to minimize these in order to improve the applicability of the model.

- (1) Both the liquid and vapor flows are assumed to be laminar. Although the model contains a check on this, according to computational results for 0.2

watts of power input to the evaporator, the maximum Reynolds number obtained for the liquid and vapor flow were 0.22 and 15.4 respectively. Both of these values are well below the range of $Re < 2000$.

- (2) The evaporation-condensation rate is assumed to be proportional to the difference between the vapor pressure and the saturation pressure and independent of the curvature of the liquid-vapor interface.
- (3) The radius of curvature for the liquid vapor interface is assumed to be a function only of the geometry of the heat pipe, the wetting angle and the liquid cross-sectional area.
- (4) The vapor within the vapor portion of the heat pipe is assumed to behave as an ideal gas. This assumption is reasonable because of the very low vapor pressures involved.
- (5) The liquid distribution within each of the four corners of the heat pipe is assumed to be uniform. Evaluation of the bond number ($B_o = \sigma_1 / \rho_1 g l^2$), which is the ratio of the viscous forces to the gravitational forces is much larger than unity for the geometry considered here. This implies that the viscous forces dominate.
- (6) Computation of the liquid-vapor interface is accomplished by treating this interface as a smooth solid boundary.
- (7) The transfer of heat at the liquid vapor interface due to conduction is assumed to be negligible.

3.2 Governing Equations

The high thermal conductivity of heat pipes is the result of the evaporation and condensation process occurring within the heat pipe and the high latent heat associated with these processes. For this reason, determination of the evaporation and condensation rate of the liquid plays a key role in determination of the heat pipe behavior. The equation for the molecular flux of evaporation, j , given by Collier (1972) was employed in this model. This relationship can be expressed as

$$j = \left(\frac{M}{2\pi RT} \right) (P_s - P_v) \quad (47)$$

where, M is the molecular weight of the fluid, R is universal gas constant, T is the absolute temperature, P_s is the saturation pressure, and P_v is vapor pressure. When P_s is greater than P_v , j is positive and the liquid evaporates.

When P_s is less than P_v , j is negative and the vapor condenses. In the numerical model, the evaporation-condensation rate is assumed to be proportional to the liquid-vapor interface area in each section of the heat pipe, i.e.

$$\Delta M_{ec} = j \Delta A_e = j w_{ec} \Delta x \quad (48)$$

where ΔA_{ec} is the evaporation-condensation surface area in one section, w_{ec} is the perimeter of the liquid-vapor interface, and Δx is the section length.

With a given latent heat, L , the rate of the heat released or absorbed in any section can be calculated by the equation

$$\Delta Q_{ec} = L \Delta M_{ec} \quad (49)$$

For the heat pipe to operate properly, the conditions existing between the capillary pressure, liquid pressure and the vapor pressure must be such that flow of the liquid back to the evaporator is promoted. This equation is the same for the micro heat pipe as for larger heat pipes and can be expressed as

$$P_{vl} = P_v - P_l = \sigma/r \quad (50)$$

where, P_v is the vapor pressure, σ is the liquid surface tension, and r is the radius of curvature of the liquid-vapor interface. Since both P_{vl} and r are functions of x , the derivative of the above equation, yields

$$\frac{dP_{vl}}{dx} = \frac{-\sigma}{r^2} \frac{dr}{dx} \quad (51)$$

For a finite interval, $dx \rightarrow \Delta x$, hence, the finite form of the equation can be expressed as

$$\Delta P_{vl} = \frac{-\sigma}{r^2} \Delta r \quad (52)$$

where

$$\Delta P_{vl} = \Delta P_{fv} + \Delta P_{mv} + \Delta P_{fl} + \Delta P_{ml} \quad (53)$$

and the pressure changes are those due to the liquid and vapor friction and the momentum changes in one section, Δx , along the heat pipe.

Based on the momentum equation, the pressure drops due to friction for laminar flow can be expressed as

$$\Delta P_f = \frac{2\mu\Delta x V}{r_h^2} \quad (54)$$

where μ is the viscosity of the fluid, r_h is the hydraulic radius, and V is the velocity of the flow and is equal to $M/\rho A$.

The pressure drop due to momentum change is given by

$$\Delta P_m = \frac{V\Delta M + M\Delta V + \Delta M\Delta V}{A} \quad (55)$$

where M is the mass flowrate and A is the flow cross-sectional area. In this model, ΔM equals ΔM_{ec} for the vapor and $-\Delta M_{ec}$ for the liquid.

The energy equation used in this model takes the form

$$Q_{in} = Q_{out} + Q_r \quad (56)$$

where

$$Q_r = \int \rho_l A_l C_{Pl} \Delta T_l dx + \int \rho_v A_v C_{Pv} \Delta T_v dx + \int \rho_s A_s C_{Ps} \Delta T_s dx \quad (57)$$

C_{Pl} , C_{Pv} and C_{Ps} are the heat capacities of the liquid, vapor and solid boundaries respectively and the ΔT 's are the corresponding temperature changes.

The continuity equation takes the form

$$\int \rho_v A_v dx + \int \rho_l A_l dx = \text{constant} = \text{fluid charge} \quad (58)$$

and total volume inside the heat pipe can be defined and expressed as:

$$\text{Vol} = \text{Vol}_l + \text{Vol}_v \text{ and } A = A_l + A_v \quad (59)$$

3.3 Modeling Approach

As is the case for larger heat pipes, the micro heat pipe also consists of three basic sections, an evaporator and a condenser, separated by an adiabatic section. Each of these sections has a different set of boundary conditions and needs to be treated accordingly. For this reason, they will be discussed separately in the following sections.

3.3.1 Evaporator Region The single boundary condition utilized in the evaporator section is the input heat density as a function of time, t , and position, x . For a given input heat density and vapor pressure at any location, x , the saturation pressure can be obtained by using the combination of molecular flux equation (47) and the energy conservation equation (57) at a given position. These equations assume the following form

$$P_s = \frac{\Delta Q_{ec}}{(M/2\pi RT_l)^{1/2} \Delta x \omega_{ec}} + P_v \quad (60)$$

$$\Delta Q_l = \frac{C_{pl} \rho A_l \Delta x \Delta T_l}{\Delta t} \quad (61)$$

$$\Delta Q_{in} = \Delta Q_{ec} + \Delta Q_l \quad (62)$$

Since T_l is a function of P_s , equations (60 through 62) can be correlated to each other. An iteration method with relaxation was used to solve the system of equations to find the value of T_l , Q_{ec} and Q_l . The difference between the boundary and liquid temperatures, ΔT_{bl} , is proportional to the input heat density. The boundary temperature can therefore be obtained by adding ΔT_{bl} to T_l .

3.3.2 Adiabatic Region. In the adiabatic section, there is by definition no heat into or out of the heat pipe. The heat absorbed by evaporation or released by condensation is equal to the heat consumed in heating up or cooling down the liquid and the heat pipe shell. The governing equations for this section therefore become

$$Q_{ec} = L\omega_{ec} \Delta x \left(\frac{M}{2\pi RT_1} \right)^{1/2} (P_s - P_v) \quad (63)$$

$$Q_l = C_{Pl} \rho_l A_l \Delta T_l \Delta x \quad (64)$$

$$Q_s = C_{Ps} \rho_s A_s \Delta T_b \Delta x \quad (65)$$

$$Q_{ec} + Q_l + Q_s = 0 \quad (66)$$

Because the magnitude of Q_{ec} in the adiabatic section is much less than that in the other two sections, the heat transferred between liquid and the heat pipe shell is very small, and hence the temperature drop can be considered negligible. By assuming $T_l = T_b$, the equations given above can be solved by iteration, to obtain Q_{ec} , Q_l , Q_s and T_l .

3.3.3 Condenser Region. In the condenser region, the boundary temperature of the heat pipe is assumed to be fixed. Therefore, the governing equations are similar to those used in the adiabatic section

$$Q_{ec} = L\omega_{ec} \Delta x \left(\frac{M}{2\pi RT_1} \right)^{1/2} (P_s - P_v) \quad (67)$$

$$Q_l = C_{Pl} \rho_l A_l \Delta T_l \Delta x \quad (68)$$

$$Q_{out} = Q_{ec} + Q_l \quad (69)$$

where ΔT_{bl} is proportional to the heat output. For a given T_b , these equations are solved for Q_{ec} , Q_l , and T_l using an iterative technique.

3.4 General Assembly

Although the heat pipe is small, many variables are involved in the determination of the transient behavior. Some of the most important ones are listed below:

A_l	-- Liquid cross-section area
A_v	-- Vapor cross-section area
M_{ec}	-- Evaporation-Condensation Rate
M_l	-- Liquid Mass Flowrate
M_v	-- Vapor Mass Flowrate
P_v	-- Vapor Pressure
P_l	-- Liquid Pressure
Q_l	-- Heat Input and Output
r	-- Radius of Curvature on Liquid-Vapor Interface
T_b	-- Boundary Temperature
T_l	-- Liquid Temperature
T_v	-- Vapor Temperature

All these parameters are functions of both x and t . In addition, most of them are interrelated and therefore solutions cannot be obtained explicitly. This serves to significantly increase the complexity of the model. A double iteration technique is employed to minimize the error. One is false position, which is used to find the root of the implicit function. The other is a relaxation technique used to find solutions for the implicit array.

Since the evaporation-condensation rate is very sensitive to changes in the vapor pressure, a special treatment is applied to obtain a stable solution. First, the evaporation rate is assumed to be equal to the condensation rate and the vapor pressure is calculated. Second, the vapor pressure is used to compute the change in the vapor mass and hence, the difference between evaporation and condensation. The original assumption of equal evaporation and condensation rates are adjusted and updated. Preliminary tests indicate that the solution is stable regardless of the time step size used. In comparison, prior to using the

predictor-corrector treatment, the solution vibrated with increasing magnitude for time step sizes below 0.0001 second.

The general computing procedures are listed below:

1. Initialize the variables and arrays.
2. Set the time equal to the first time step.
3. For a given boundary condition, compute the boundary, liquid and vapor temperatures and the evaporation-condensation rate for each section by assuming that the total evaporation equals the total condensation.
4. Compute the pressure drops and flowrates for each section by iteration.
5. Compute the radii of curvature for the liquid-vapor interface.
6. Compute the vapor pressure along with the boundary, liquid and vapor temperatures and the evaporation-condensation rate for each section by iteration.
7. Make a correction on the liquid-vapor mass change using the predicted vapor pressure.
8. Repeat steps 4 through 6 with the vapor pressure correction.
9. Calculate the liquid and vapor flowrate once again with the corrected vapor pressure. Calculate the liquid pressure.
10. Renew all of the variables and arrays and print out the results.
11. If the time is less than the given limit, increase on time step and go back to step 2.

3.5 Discussion of the Transient Modeling Results

3.5.1 Geometry. Because both the steady-state and transient performance of the heat pipe are strongly dependent upon the physical geometry, it is necessary to accurately describe this geometry. The actual shape, shown in Fig. 8, the shape can be described as follows

$$a = \frac{d_d}{2} \cos \frac{\pi}{4} \quad (70)$$

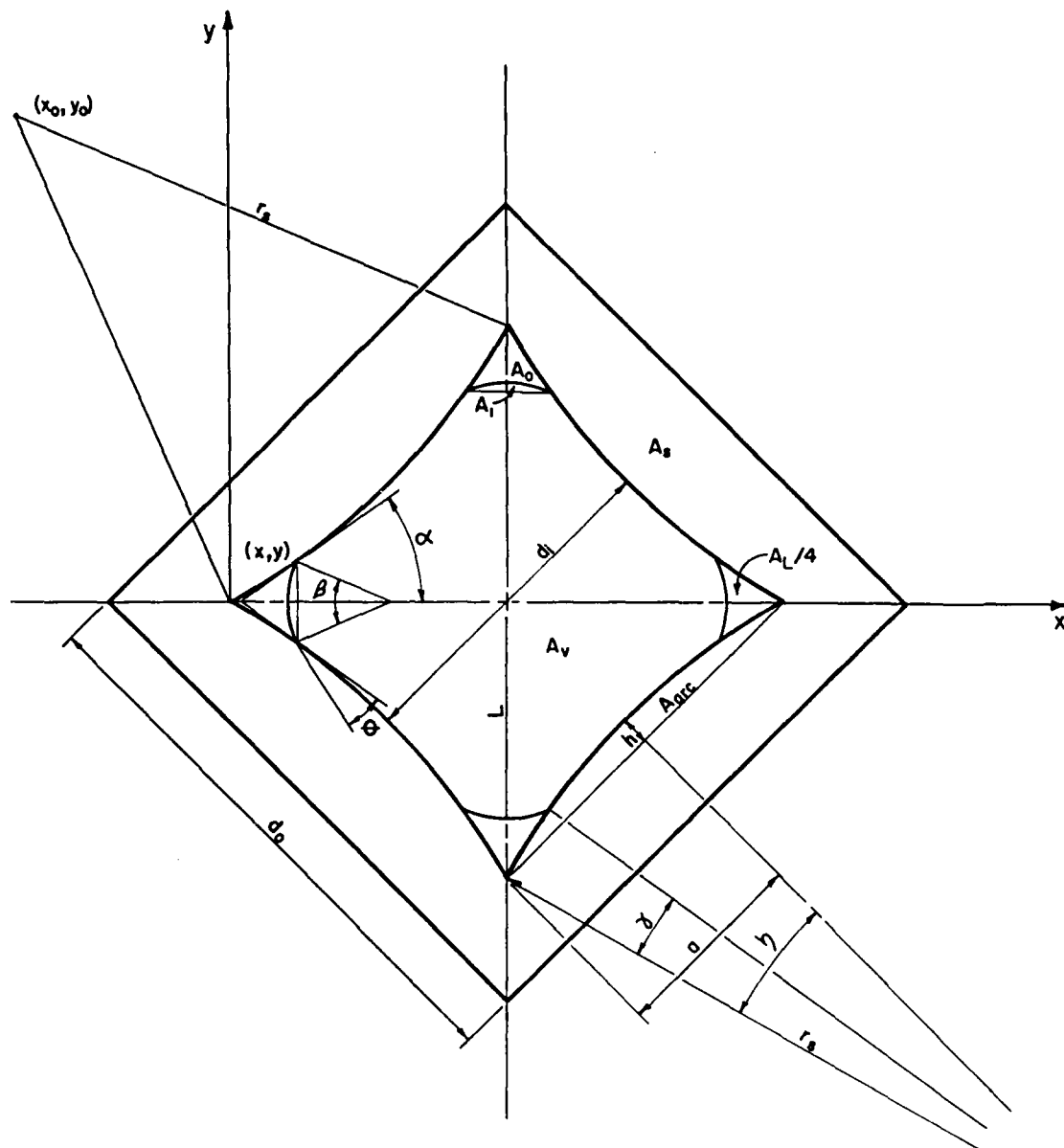


Fig. 8 Dimensional nomenclature for the trapezoidal heat pipe transient model.

$$h = a - \frac{d_i}{2} \quad (71)$$

$$r_s = \frac{a^2 + h^2}{2h} \quad (72)$$

$$\eta = \sin^{-1} (a/r_s) \quad (73)$$

$$x_0 = -r_s \sin (\pi/4 - \eta) \quad (74)$$

$$y_0 = r_s \cos (\pi/4 - \eta) \quad (75)$$

$$y = y_0 - \sqrt{r_s^2 - (x - x_0)^2} \quad (76)$$

$$A_{\text{arc}} = r_s^2 (\eta - \sinh \eta \cosh \eta) \quad (77)$$

$$A = (d_d \sin \pi/4)^2 - 4A_{\text{arc}} \quad (78)$$

$$A_s = d_o^2 - A \quad (79)$$

$$\frac{dy}{dx} = \frac{x - x_0}{\sqrt{r_s^2 - (x - x_0)^2}} \quad (80)$$

$$\alpha = \tan^{-1} (dy/dx) \quad (81)$$

$$\beta_0 = \pi - 2\alpha \quad (82)$$

$$\beta = \beta_0 - 2\theta \quad (83)$$

$$\gamma = 2 \sin^{-1} \frac{\sqrt{x^2 + y^2}}{2r_s} \quad (84)$$

$$r = \frac{y}{\sin (\beta/2)} \quad (85)$$

$$A_0 = 2 \left\{ y_0 x - \frac{(x - x_0)}{\sqrt{(r_s^2 - (x - x_0)^2)}} - x_0/2 \sqrt{(r_s^2 - x_0^2)} + \frac{r_s^2}{2(\sin^{-1}(-x_0/r_s) - \sin^{-1}(x-x_0)/r_s)} \right\} \quad (86)$$

$$A_1 = \frac{\beta r^2}{2} - y \sqrt{r^2 - y^2} \quad (87)$$

$$A_1 \approx A_0 - A_1 \quad (88)$$

$$\omega p_1 = 2\gamma r_s + r\beta \quad (89)$$

$$\omega p_{ec} = 4r\beta \quad (90)$$

$$\omega p_v = 8r_s (\eta - \gamma) + 4r\beta \quad (91)$$

with restrictions

$$d_i \leq \frac{\sqrt{2}}{2} d_d \quad (92)$$

$$d_d < \sqrt{2} d_o \quad (93)$$

The dimensions obtained for the pipe tested were $d_o = 1.0$ mm, $d_i = 0.6$ mm, and $d_d = 1.0$ mm.

Once the geometry was known, it was necessary to determine the contact angle, θ , which was computed as:

$$\theta = \cos^{-1} \left(\frac{\sigma_{sv} - \sigma_{sl}}{\sigma_{lg}} \right) \quad (94)$$

Although some information is available on the surface tension between the solid and the liquid, σ_{sl} , only limited information on the other two values, the

surface tension between the solid and the vapor, σ_{sv} , and the liquid and the vapor, σ_{lv} , was available. For this reason, an experimental investigation was conducted to determine the contact angle between copper and water, and also between silver and water.

An acrylic chamber with internal dimensions of approximately 2.54 cm by 2.54 cm by 8.0 cm was constructed. The front and back walls of the chamber were transparent while the left and right sides were made of copper and silver respectively. The chamber was filled through a fill port located in the top, with approximately 10 cm³ of distilled water. The chamber was evacuated for approximately 5 minutes to eliminate noncondensable gases. The fill port was then closed, sealing the chamber. By tilting the chamber until the liquid at the interface formed a flat surface as shown in Fig. 9, the contact angle could be measured. The results of these experimental measurements indicated contact angles of 55° and 45° for copper and silver respectively.

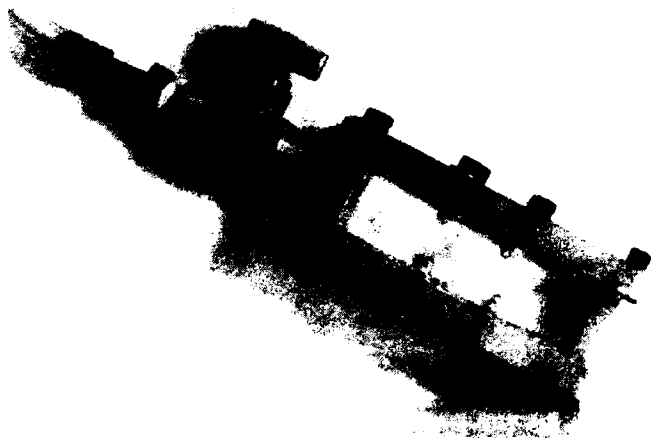


Fig. 9 Photograph of the contact angle experimental device.

The preliminary results from the numerical model indicated that this parameter, the contact angle, was of significant importance in determining the liquid pressure drop, the maximum capillary pumping pressure, the maximum heat transport capacity, and the time required to reach steady-state.

Figure 10 compares the liquid cross-sectional area with the liquid-vapor interfacial pressure drop for wetting angles of 0° and 45° . As illustrated, the maximum liquid cross-sectional area for a contact angle of 45° is 0.218 mm^2 , much larger than the 0.116 mm^2 for a contact angle of 0° . As a result, the difference between the minimum interface curvature in the evaporator and the maximum interface curvature in the condenser is much larger for the 45° contact angle than for the case of the 0° contact angle for the same heat input, as illustrated in Fig. 11. Near dryout, the frictional pressure drop in the evaporator is much larger for the 45° contact angle than for the 0° case as illustrated in Fig. 12. The resulting effects of variations in the contact angle are large differences in the liquid pressure drop and the capillary pumping pressure.

The relationships described above do not necessarily mean that large contact angles will result in a larger maximum heat transport capacity, since the heat transport capacity is also dependent upon the liquid charge within the heat pipe. Using the fill charge of the actual test pipes, and a 31°C condenser bath temperature, a maximum heat transport capacity of 0.11 watt for a 45° contact angle resulting from evaporator dryout was predicted as compared to a maximum value of 0.12 for a 0° contact angle resulting from condenser flooding. In addition to affecting the pressure drops, the transient analysis indicates that the time required for the heat pipe to reach steady-state is longer for larger contact angles. Once a heat input of 0.1 watt has been reached, a total of 80 seconds is required for the heat pipe to reach steady-state for contact angles

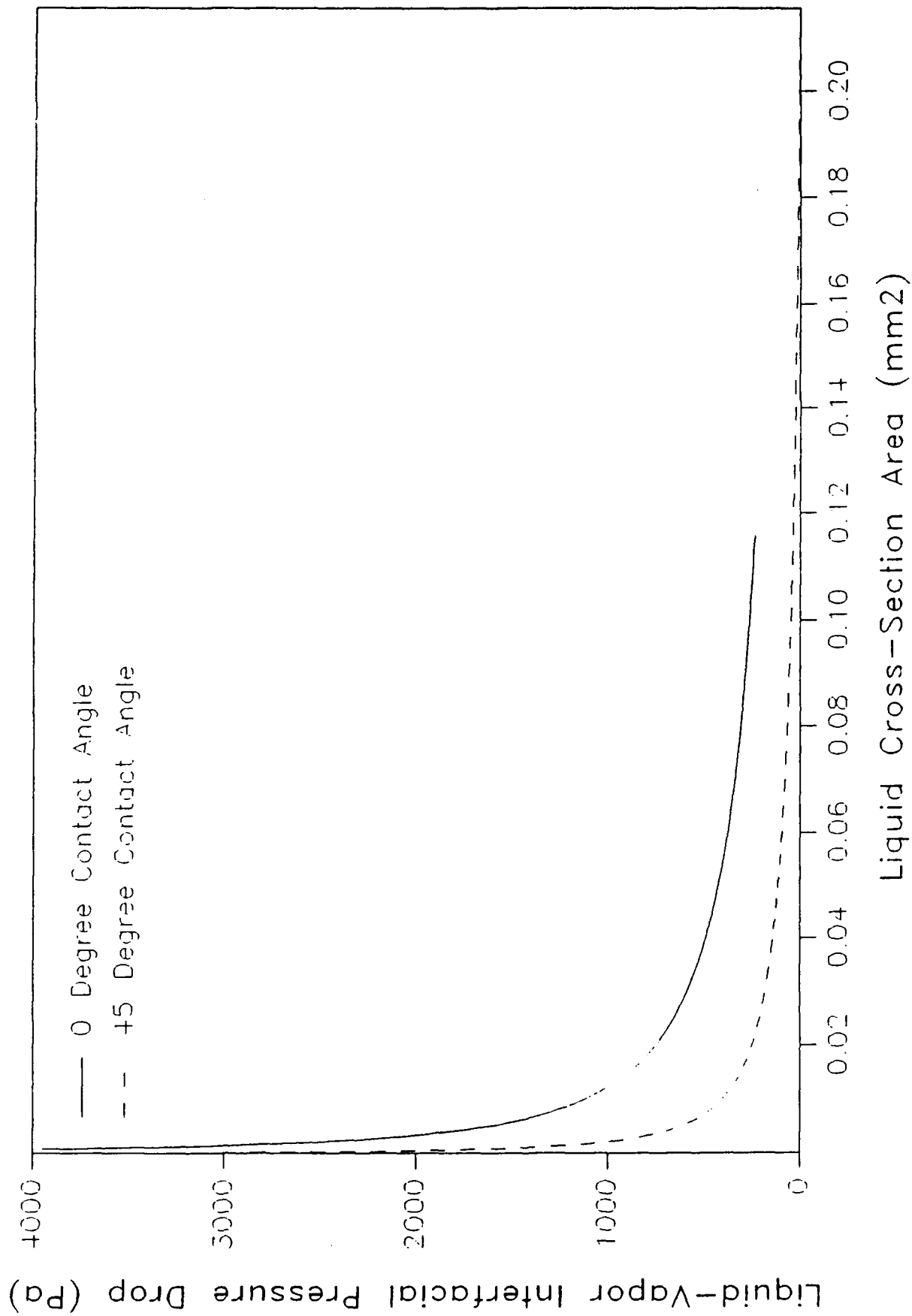


Fig. 10 Comparison of the interfacial pressure drop as a function of the liquid cross-sectional area.

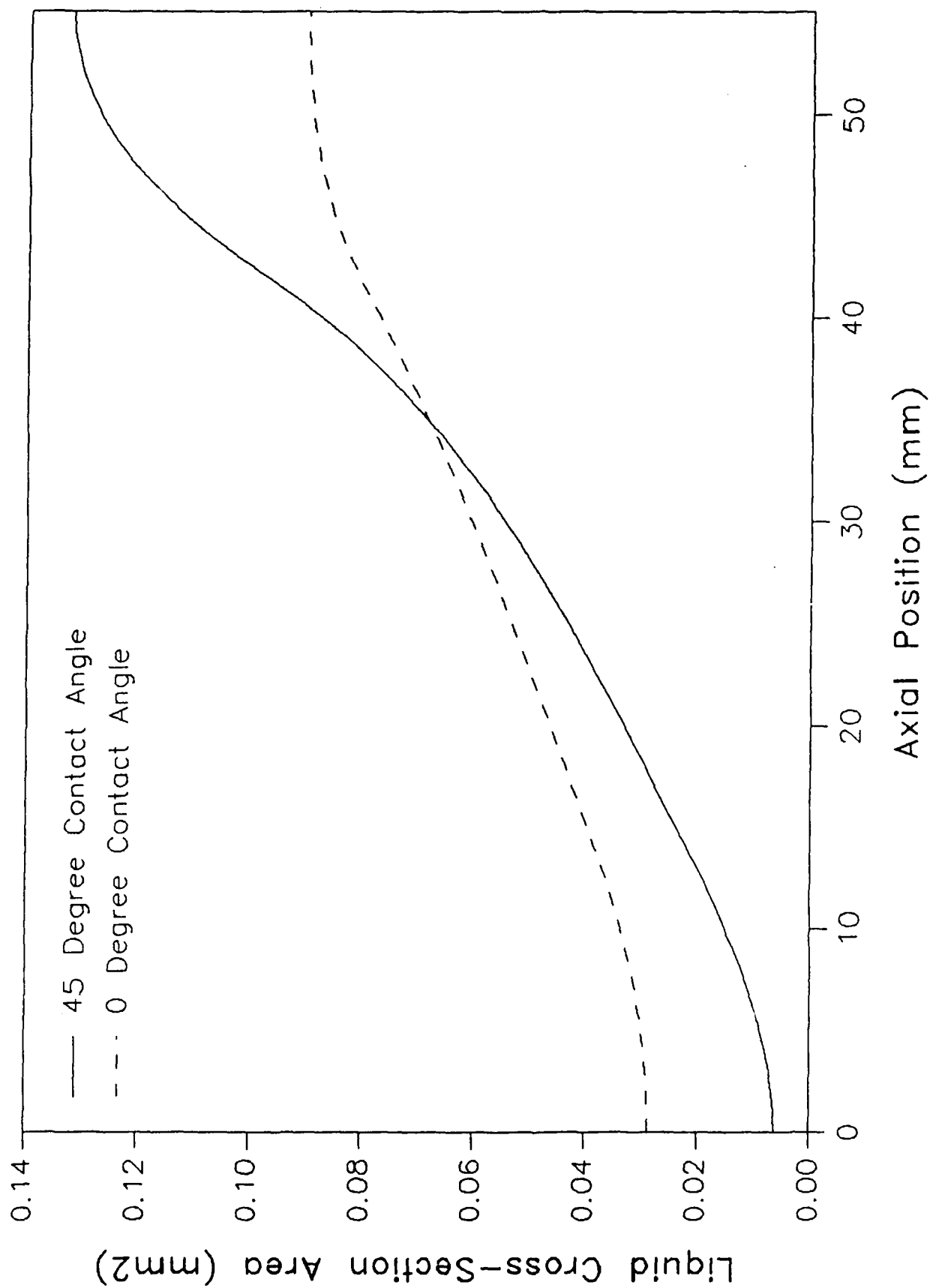


Fig. 11 Steady-state liquid cross-sectional area as predicted by the transient model.

of 45° , while only 30 seconds are required if the contact angle is 0° .

Because of the geometrical shape of the heat pipe, a phenomena referred to as an inverted meniscus occurs at contact angles greater than 45° . This phenomena can best be described as a change in the shape of the liquid-vapor interface from one that is convex to one which is concave. From the above analysis, it is apparent that the contact angle is one of the key parameters in the determination at the optimum charge and the heat transport capacity of the heat pipe.

The steady-state temperature profile as predicted by the transient model is illustrated in Fig. 13 for an input power of 0.1 watt and a contact angle of 45° . As shown, the liquid, vapor, and boundary temperatures are all the same at the left end of the pipe. This point represents the highest temperature within the pipe. The vapor temperature decreases slightly in the evaporator region and then remains essentially constant throughout the adiabatic and condenser regions. The boundary and liquid temperatures decrease somewhat more rapidly in the evaporator region and continue to decrease in both the adiabatic and condenser regions. The two large gradients are apparent at the exit to the evaporator and the entrance to the condenser and are the result of longitudinal step size used in the model. Because the wall of the heat pipe is very thin, the temperature difference between the wall and the liquid temperatures are very small.

The transient model indicates that the vapor temperature variations are proportional to the heat input, and that without dryout or flooding, the conductivity of the heat pipe is close to a constant value with respect to time. In contrast to the vapor temperature, a fairly long period of time is required for the other thermal hydraulic parameters to reach their steady-state values. The time period for the case mentioned previously ranges from 30 seconds to 80

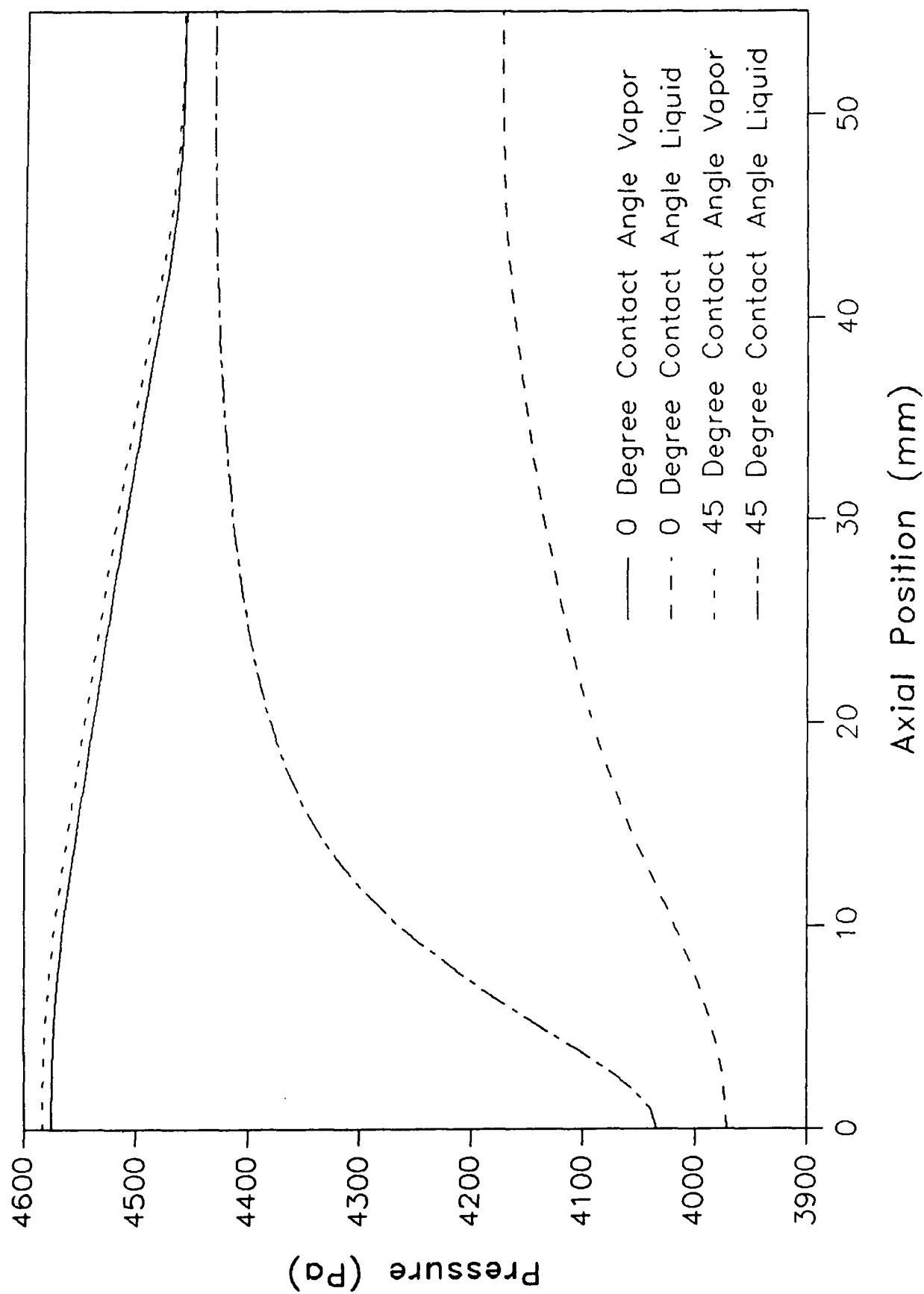


Fig. 12 Steady-state liquid and vapor pressure as a function of position as predicted by the transient model

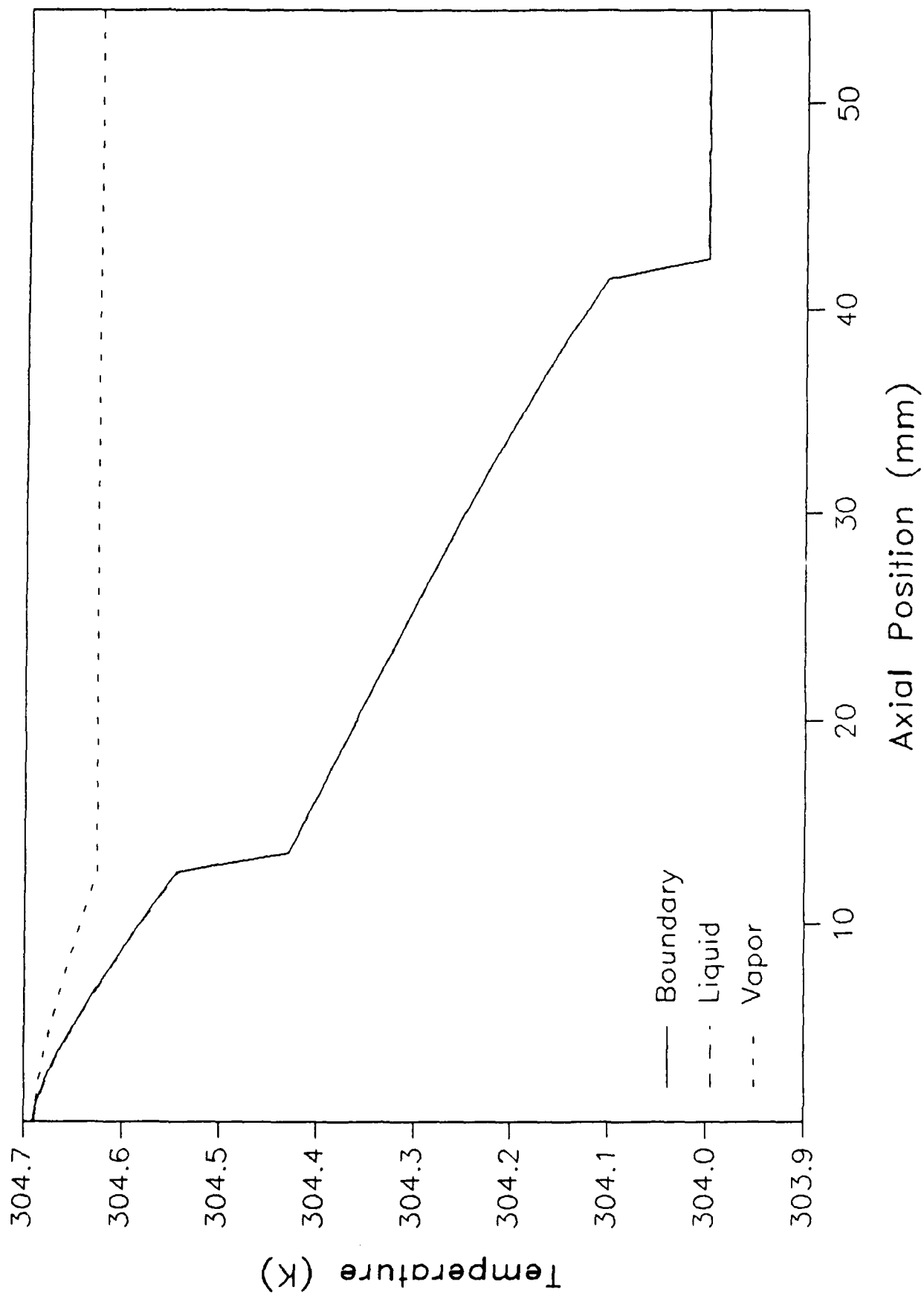


Fig. 13 Steady-state temperature distribution as predicted by the transient model.

seconds after full heat input, depending on the contact angle. The smaller the contact angle and the higher the temperature, the shorter the time required.

Figures 14 and 15 illustrate the changes in the liquid mass flow rate and liquid cross-sectional area as a function of time. It is significant to note that during the time immediately after the application of the heat to the evaporator, the liquid and vapor flow in the evaporator are both in the same direction. This reverse liquid flow is the result of an imbalance in the total pressure drop. The evaporation rate does not provide a change in the liquid-vapor interfacial curvature, adequate to compensate for the total pressure drop resulting from the temperature change. Once the heat input reaches full load the reverse liquid flow disappears and the liquid mass flow rate gradually increases until it reaches a steady-state condition in which the liquid mass flow rate is equal to the vapor mass flow rate in any given section. This is more apparent in Fig. 16 which illustrates the pressure as a function of axial position for both 10 seconds after start-up and for steady-state. As illustrated, at 10 seconds after start-up, the pressure of both the liquid and vapor are higher in the evaporator and gradually decrease with position, promoting flow away from the evaporator, while at steady-state, the liquid pressure is much lower in the evaporator and increases dramatically with position, promoting flow back to the evaporator.

Finally, it is important to note that the pressure drops due to friction are much larger than for either the pressure drops due to the vapor momentum change (two orders of magnitude) or the pressure drop due to the liquid momentum change (four orders of magnitude).

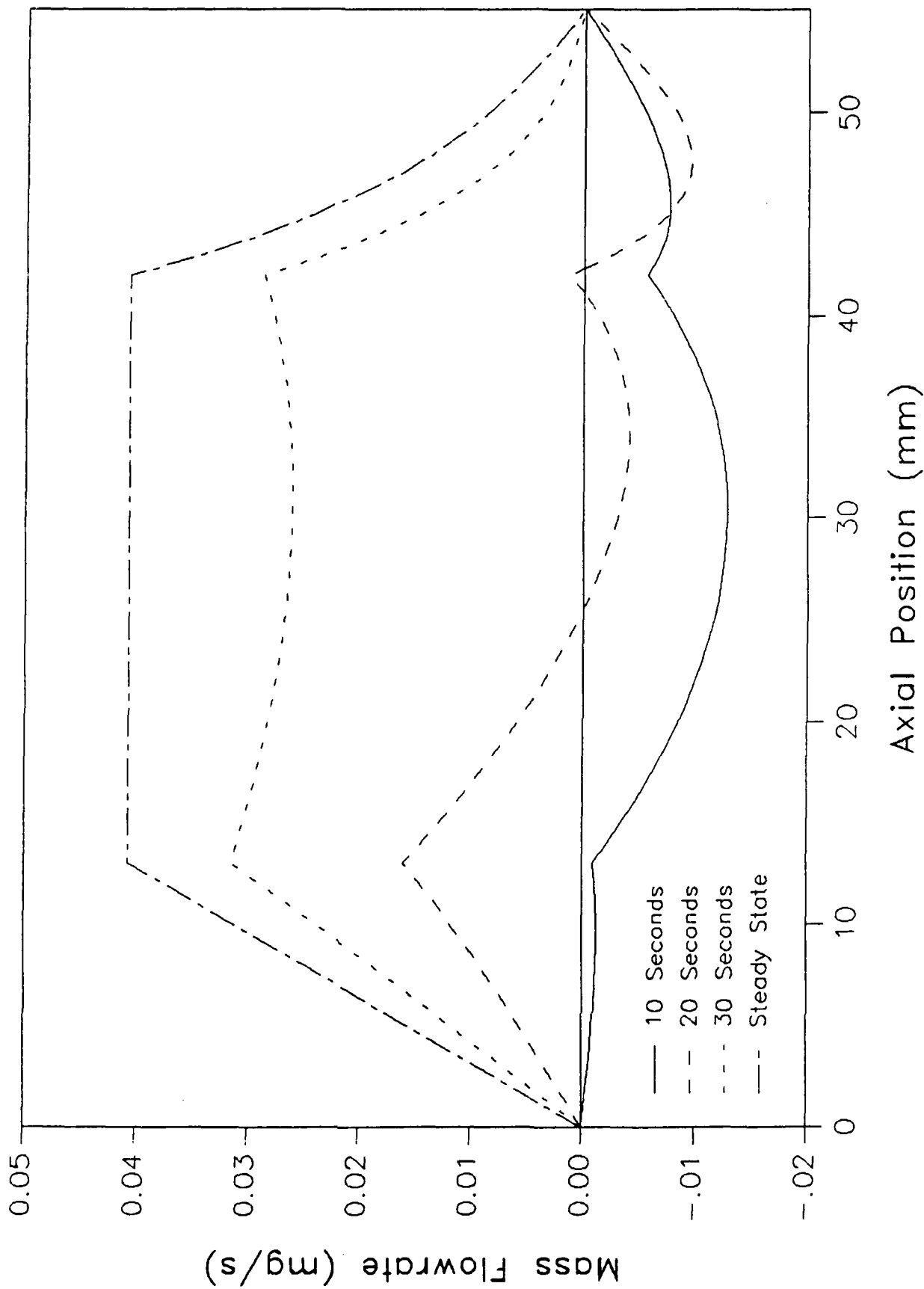


Fig. 14 Liquid mass flow rate as a function of time and the axial position.

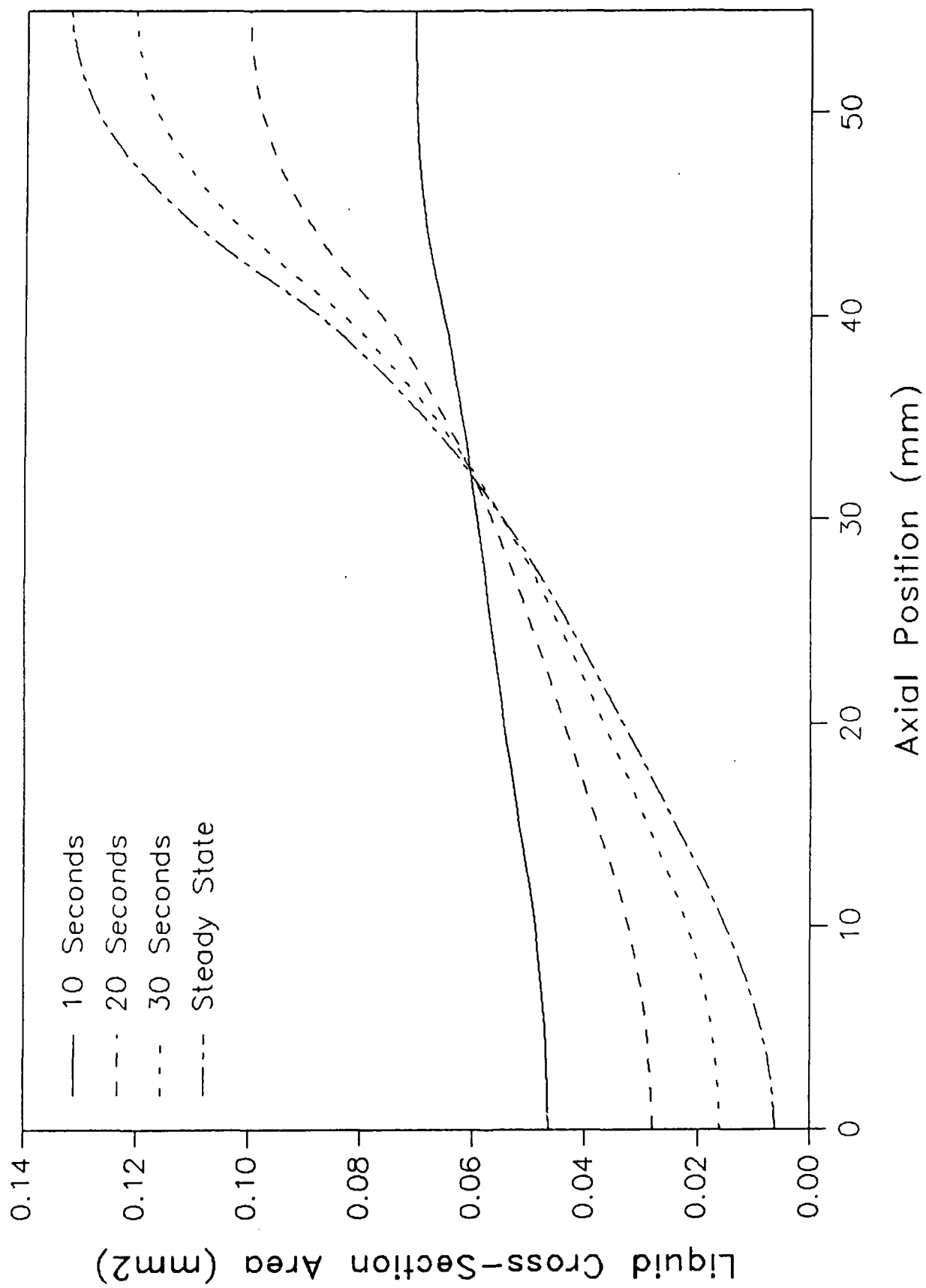


Fig. 15 Liquid cross-sectional area as a function of time and the axial position.

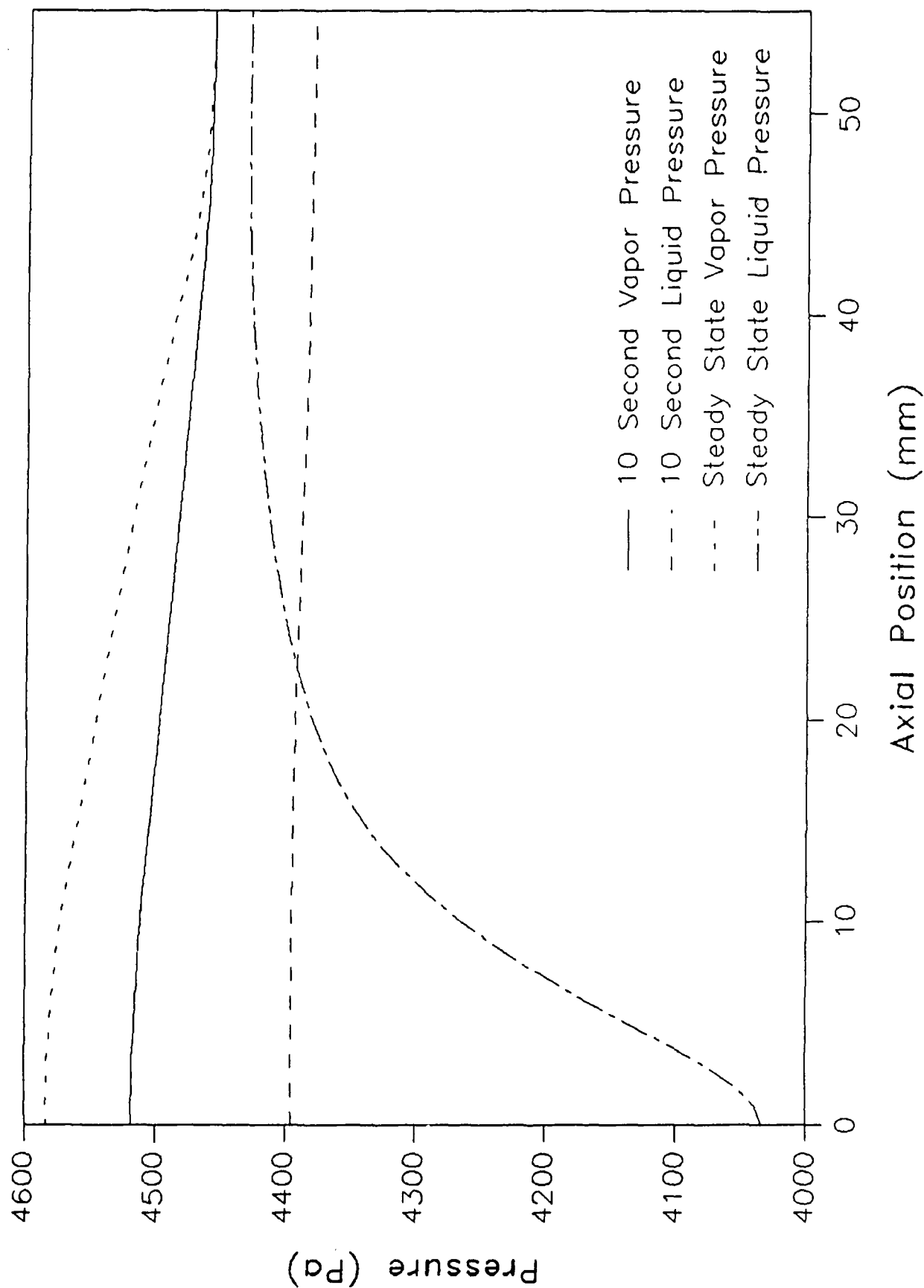


Fig. 16 Liquid and vapor pressure as a function of time and the axial position.

IV. EXPERIMENTAL PROGRAM

4.1 Description of Test Article

The test articles used in this investigation were obtained from ITOH Research and Development Corporation of Japan. The physical size and internal dimensions are illustrated in Figs. 1 and 2 respectively. As shown, the outer dimensions are 1 mm by 1 mm and the length is 57 mm. The case material was either copper or silver and the working fluid used was ultrapure water. Two of the test pipes, one silver and one copper, were charged with 0.0032 gram of fluid prior to sealing. Two additional uncharged test pipes were also obtained to establish a baseline value and determine the improvement in the heat transport capacity due to the vaporization and condensation.

4.2 Description of Experimental Apparatus

To conduct the experimental portion of the investigation, a test facility was constructed in the Conduction Heat Transfer Laboratory at Texas A&M University. This test facility illustrated in Fig. 17, consisted of five

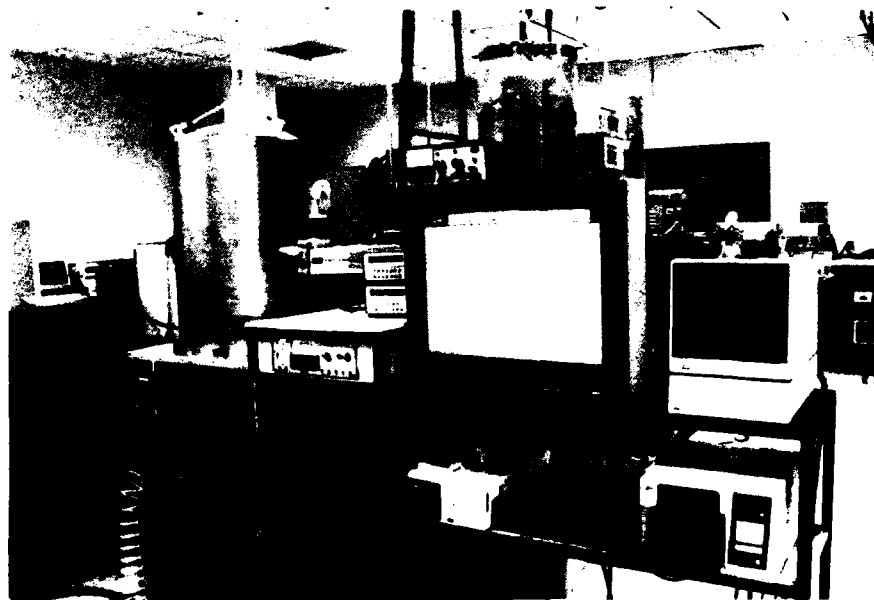


Fig. 17 Photograph of the micro heat pipe test facility with the IR camera.

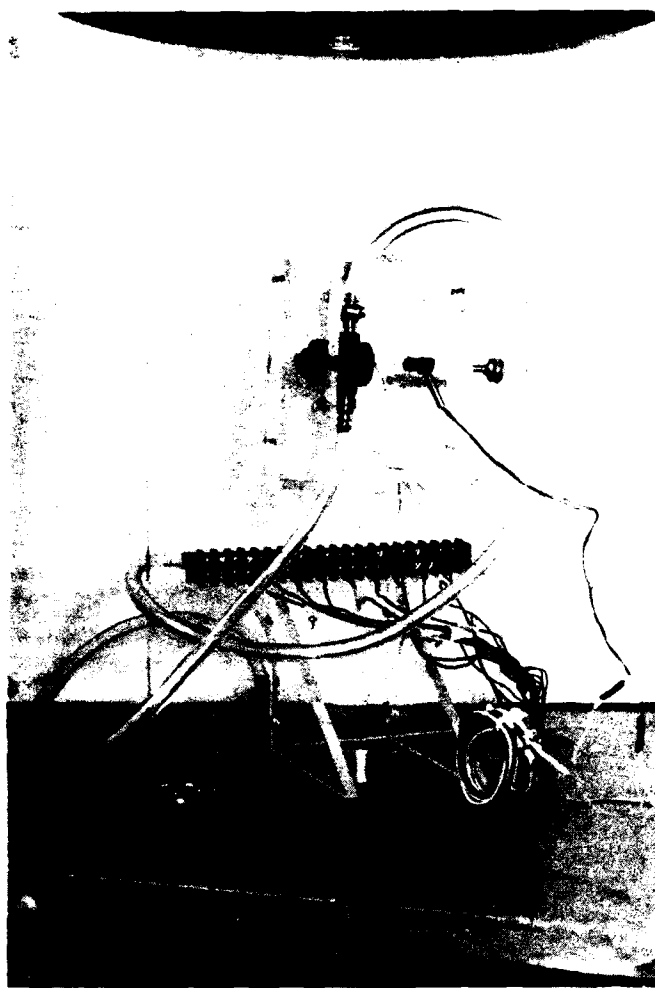


Fig. 18 Micro heat pipe test stand.

subsystems: the test stand, a variable heat source, a constant temperature cooling source, a data acquisition system, and a vacuum system. The test stand, shown in Fig. 18, was constructed from Plexiglass and allowed the micro heat pipe to rotate through an angle of 360° . This allowed testing at tilt angles which both helped and hindered the return of liquid back to the evaporator. The test stand also supported an aluminum cooling chamber which surrounded the condenser region of the heat pipe. A Forma Scientific circulating bath provided a constant temperature fluid to the cooling chamber where it flowed over the condenser portion of the heat pipe. The bath was controlled in such a manner that a coolant, consisting of an ethyl glycol solution of constant temperature and flow rate was continually provided.

The evaporator portion of the heat pipe was surrounded by a piece of solid copper 0.635 cm in diameter and 1.27 cm in length. This copper heat spreader was in turn encased in an electric resistance heater manufactured by Watlow Manufacturing Company. The power was controlled by a regulated power supply and monitored by measuring the voltage and current to the resistance heater.

Two separate techniques were used to monitor the temperature distribution of the heat pipe. The first of these consisted of a series of Chromel-Alumel K-type thermocouples attached to the outer wall of the heat pipe. Three thermocouples were located at equidistant positions on the evaporator portion of the heat pipe: one at the end of the pipe, one at the end of the evaporator portion, and one midway between. Two additional thermocouples were located in the condenser region: one on the outer surface of the heat pipe at the entrance to the condenser, and the other located at the entrance to the condenser bath. In addition, one thermocouple was located on the outer surface of the heater for use in calibration. The thermocouples were monitored using an HP 3497A data acquisition system in conjunction with an HP 87XM Personal Computer which monitored not only the temperatures but the voltage and current measurements as made by two HP 3478A multimeters.

The second technique used to monitor the temperature distribution in the heat pipe was an infrared thermal measurement system. A Hughes Probe Eye TVS Model 3000 Infrared Camera in conjunction with an RGB Monitor and a Real Time Recorder were used to observe the test pipe during both start-up and steady-state operation. Using this system the temperature distribution along the heat pipe could be measured with an accuracy of $\pm 0.05^{\circ}\text{C}$.

To reduce any heat losses through convection, all of the tests were conducted in a vacuum of $> 10^{-2}$ torr. The entire test facility was encased in a stainless steel vacuum chamber equipped with a single crystal silicon window

which allowed observation with the thermal measurement system. A mechanical roughing pump in series with an oil diffusion pump were used to obtain the required vacuum.

4.3 Experimental Procedure

To fully understand the operational characteristics and performance limitations of the heat pipe, we developed an experimental test plan comprised of two tasks:

- i. Testing of a charged copper pipe to determine the time required for the heat pipe to reach steady-state.
- ii. Testing of several charged pipes, one copper and one silver, to obtain data with which to determine the accuracy of the steady-state and transient model (at steady-state); to determine the maximum steady-state transport capacity; and to determine the effect of variations in the type of case material used and the fluid contact angle.

To accomplish these tasks, an experimental procedure was developed and used in all of the measurements made. This procedure can be described as follows: once the heat pipe had been instrumented with the thermocouples, fitted with the evaporator heat sink and condenser, and mounted on the fixture, the heat pipe, evaporator, and condenser were all painted with a flat black paint of known emissivity to enhance the IR resolution. The test fixture was placed in the vacuum chamber and the constant temperature bath adjusted to the desired temperature. The bell jar was lowered and the vacuum pump was turned on. The heat pipe and the test facility were allowed to outgas for a minimum of 12 hours.

Once the desired vacuum had been obtained, the input heat flux was increased in small increments until the desired operating temperature had been reached. Adequate time was allowed between each incremental increase to allow the heat pipe to stabilize. When the desired operating temperature had been reached, the heat addition continued until steady-state was reached (approximately 20 minutes

as illustrated in Fig. 19) at which time the experimental data, including the time, date, power level, thermocouple temperatures, and coolant bath temperature were recorded. For the transient data shown in Fig. 19 and for several steady-state tests, the thermal history of the pipe, as measured by the IR thermography system, was also recorded.

To obtain the data for the next successive operating temperature, the heat flux was incremented and the temperature of the coolant bath adjusted to maintain a constant temperature at the entrance to the heat pipe condenser. This procedure was followed until the conductance of the heat pipe approached a constant value. At this time, the temperature of the coolant bath was incremented, and the process was repeated for a new operating temperature.

V. RESULTS

Figure 19 compares the evaporator temperature with the elapsed time for two different power increments. As shown, the heat pipe reaches steady-state, for both power levels quite rapidly, with the time required increasing with the size of the power level increment. Using these data, a time of 1,200 seconds (20 minutes) was established as the minimum acceptable time between readings. This ensured that the heat pipe would always be operating at steady-state when data were recorded and helped to accelerate the testing process by eliminating the need to continually monitor the heat pipe for temperature changes.

Figure 20 illustrates the results obtained for a copper heat pipe of the dimensions shown in Figs. 1 and 2, operating in a horizontal orientation and charged with 0.0032 gm of ultrapure water. The heat pipe was evaluated at a total of six different operating temperatures: 30.8°C, 39.5°C, 43.8°C, 51.6°C, 58.9°C, and 67.6°C. The conductance value shown as the vertical axis was computed based upon the input power to the pipe as measured by the two multimeters. It is important to note the magnitude of the parameters compared

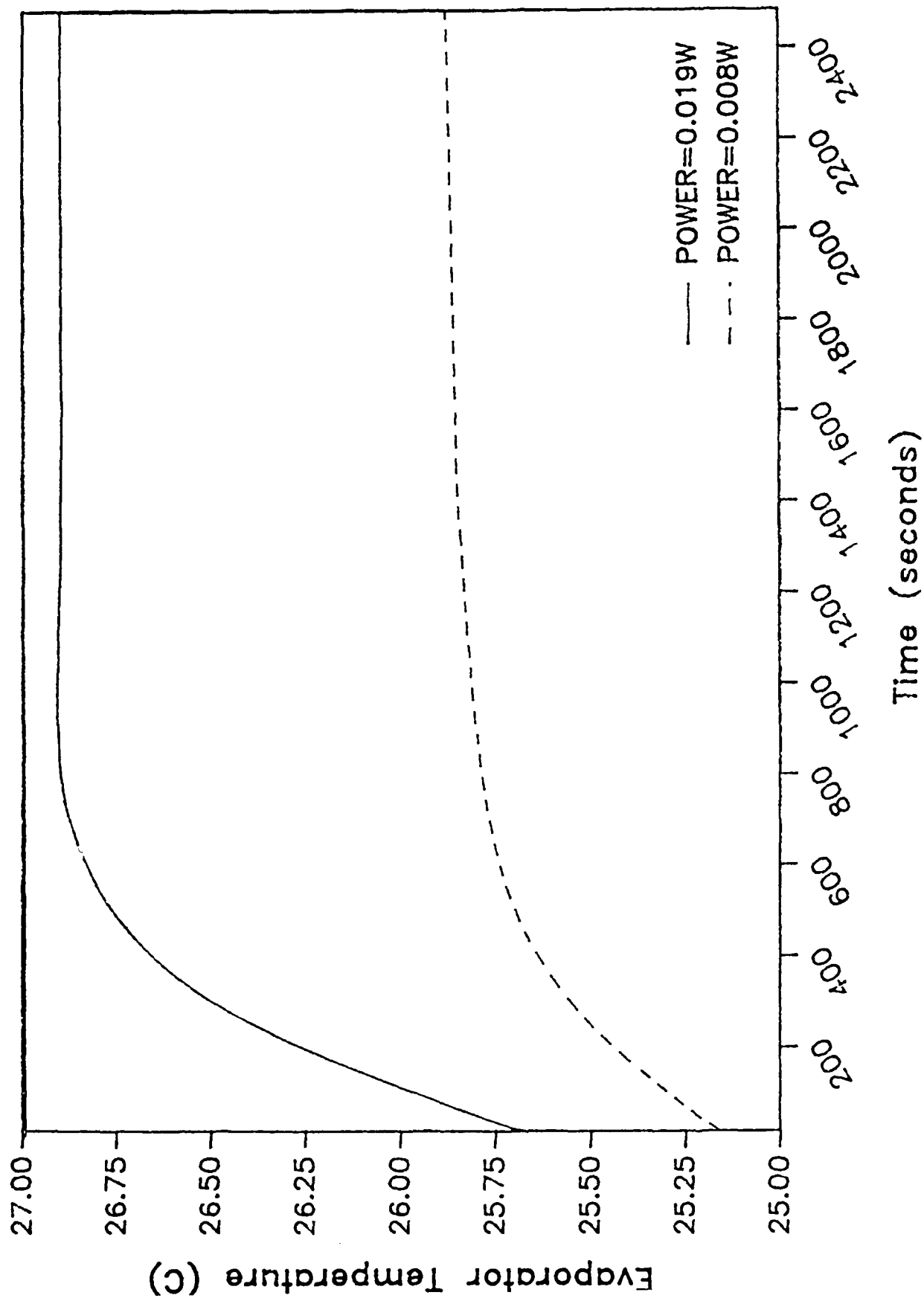


Fig. 19 Experimental determination of the time required to reach steady-state at different power levels.

in this figure. Although the variations in the thermal conductance, shown on the ordinate, appear very large, in reality they are quite small compared to the changes in operating temperature.

As illustrated in Fig. 20, the thermal conductance of the pipe decreased rapidly with respect to the evaporator temperature and asymptotically approached a constant value somewhat above the theoretical value for an uncharged pipe. The conductance value then decreased only slightly with increases in the input power. With the exception of the constant difference between the ultimate conductance value of the test pipe and the theoretical conductance of the uncharged pipe, this behavior is precisely what would be expected for a heat pipe in which the evaporator is slowly drying out.

The constant difference between the ultimate conductance value of the test pipe and the theoretical conductance of the uncharged pipe, can be explained as follows: increases in the input power initially cause the liquid meniscus to recede into the liquid channels located in the corners of the heat pipe. This results in a decrease in the radius of curvature of the liquid-vapor meniscus, a corresponding decrease in the cross-sectional area of the liquid and hence, a slight increase in the evaporator temperature (all of which are apparent from the results of the transient model, Figs. 11, 15, and 16). The recession of the meniscus continues until dryout of the evaporator occurs. Once the evaporator begins to dry out, the conductance of the test pipe rapidly approaches the conductance of an uncharged pipe as shown in Fig. 20. Although the tendency is the same for all six operating temperatures, the approach toward the uncharged pipe value is gradual. This gradual approach is the result of an increase in the effective size of the evaporator. As described previously, the heat is supplied to the heat pipe by an electrical resistance heater wrapped around 1.27 cm of the heat pipe. Prior to dryout, all of the evaporation occurs over this

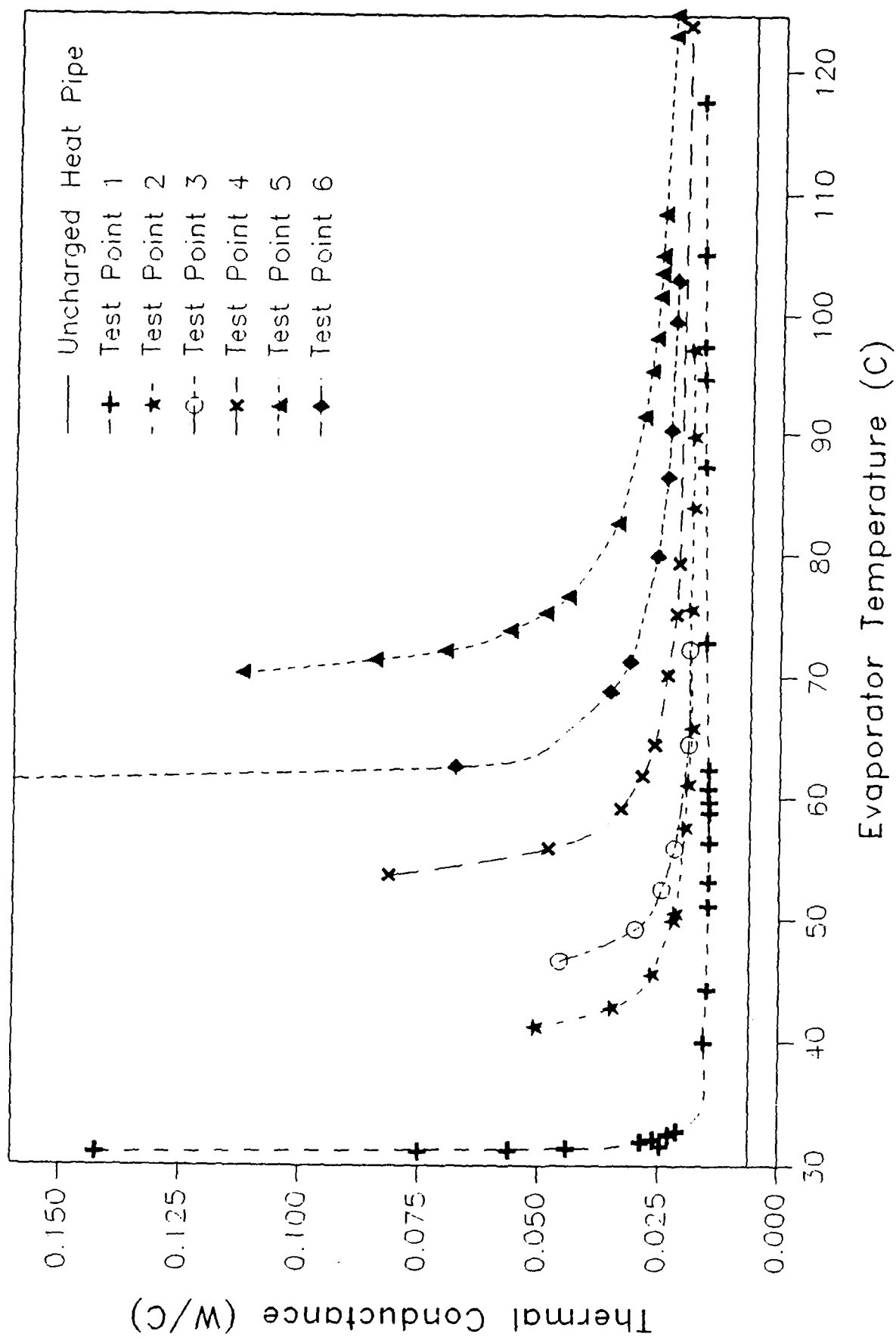


Fig. 20 Measured thermal conductance of a trapezoidal micro heat pipe as a function of the evaporator temperature (copper, 0.0032 gm charge).

region. Once dryout begins, the temperature of the heat pipe case in the adiabatic section increases, and a small part of what was formerly the adiabatic section begins to act as an evaporator. As the power continues to increase, the dryout in the evaporator spreads and the portion of the adiabatic section which behaves as an evaporator also expands. In the extreme case where complete dryout of the evaporator section occurs, a large portion of the adiabatic section may behave as an evaporator and may even begin to dry out at the end farthest from the condenser.

Figure 21 illustrates the results obtained for a silver heat pipe of the same dimensions, charged with 0.0032 gm of ultrapure water and operating under similar conditions. In this case, however, the operating temperatures at which the heat pipe was evaluated were 31.8°C, 32.3°C, 42.0°C, 52.2°C, and 62.8°C. As shown, the trends and tendencies are all similar to those of the copper pipe tested.

5.1 Comparison of Analytical and Experimental Results

To compare the results of the experimental investigation with those predicted by the analytical model, it was necessary to develop a method for determining the point at which dryout begins. The experimental data presented in Figs. 20 and 21, clearly display a change in the operation of the heat pipes as the operating temperature and power levels were increased. After reviewing the experimental data, we attempted to identify and better quantify the onset of the dryout condition. Because of the expansion of the evaporator portion into the adiabatic section of the heat pipe described previously, this proved to be quite difficult.

Several strategies were employed, including development of a mathematical method for determining the maximum curvature for each operating temperature. The final approach used was to select a region on both sides of the point of

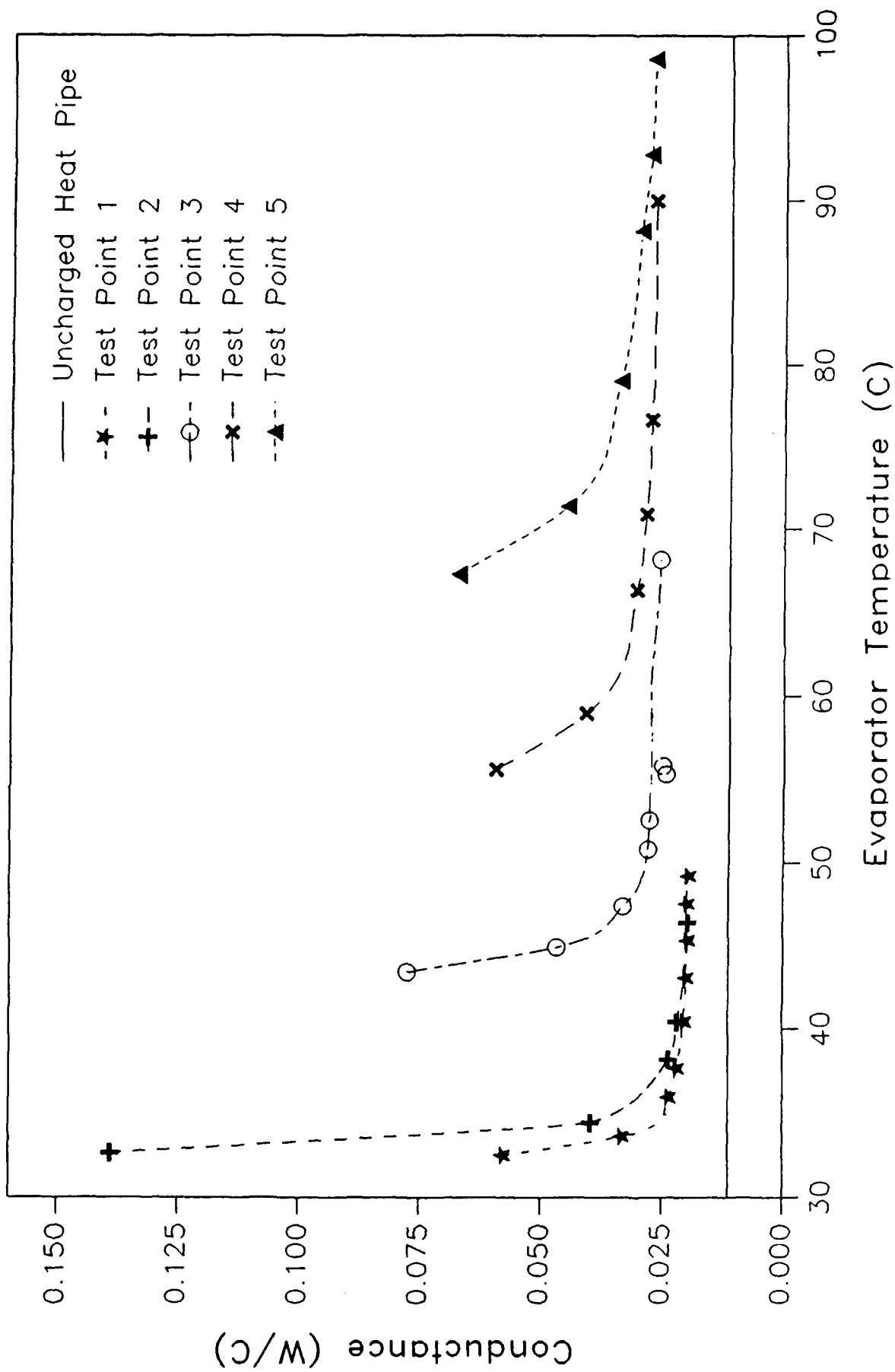


Fig. 21 Measured thermal conductance of a trapezoidal micro heat pipe as a function of the evaporator temperature (silver, 0.0032 gm charge).

maximum curvature, that is a range around the point at which the most rapid change of the conductance occurs with respect to evaporator temperature. This range was assumed to be the region over which dryout occurred.

The initial point, which will be referred to as the onset of dryout was identified as that point where the slope of the curve was 60 degrees. The termination of dryout was assumed to occur at that point where slope of the curve was 30 degrees. Although this would appear to be a large range, in reality it is probably reasonably close to the actual behavior since dryout is a gradual process and unlike boiling, develops quite slowly.

Figures 22 and 23 illustrate the results of this process and compare the experimentally determined maximum heat transfer capacity with those predicted by the steady-state and transient models for the copper and silver test pipes respectively. When the the condenser temperature was increased to temperatures above ambient, a small amount of power was required to maintain a uniform temperature along the pipe. To determine the maximum heat transfer capacity, shown on the vertical axis, this initial power was subtracted from the actual power input as measured by the multimeters.

As shown in Figs. 22 and 23, when the steady-state experimental results were compared with the analytical model, they verified the modeling predictions for both the steady-state model and the transient model (at steady-state). The steady-state model overpredicted the experimentally determined maximum heat transport capacity by approximately 30 percent for both the copper and silver test pipes. The transient model (at steady-state), however, proved to be significantly more accurate with the difference between the measured and predicted values averaging less than 10 percent for the copper test pipe and 5 percent for the silver test pipe. If a value for $H(L)$ is used in the model developed by Cotter (1984), it predicts the onset of dryout reasonably well,

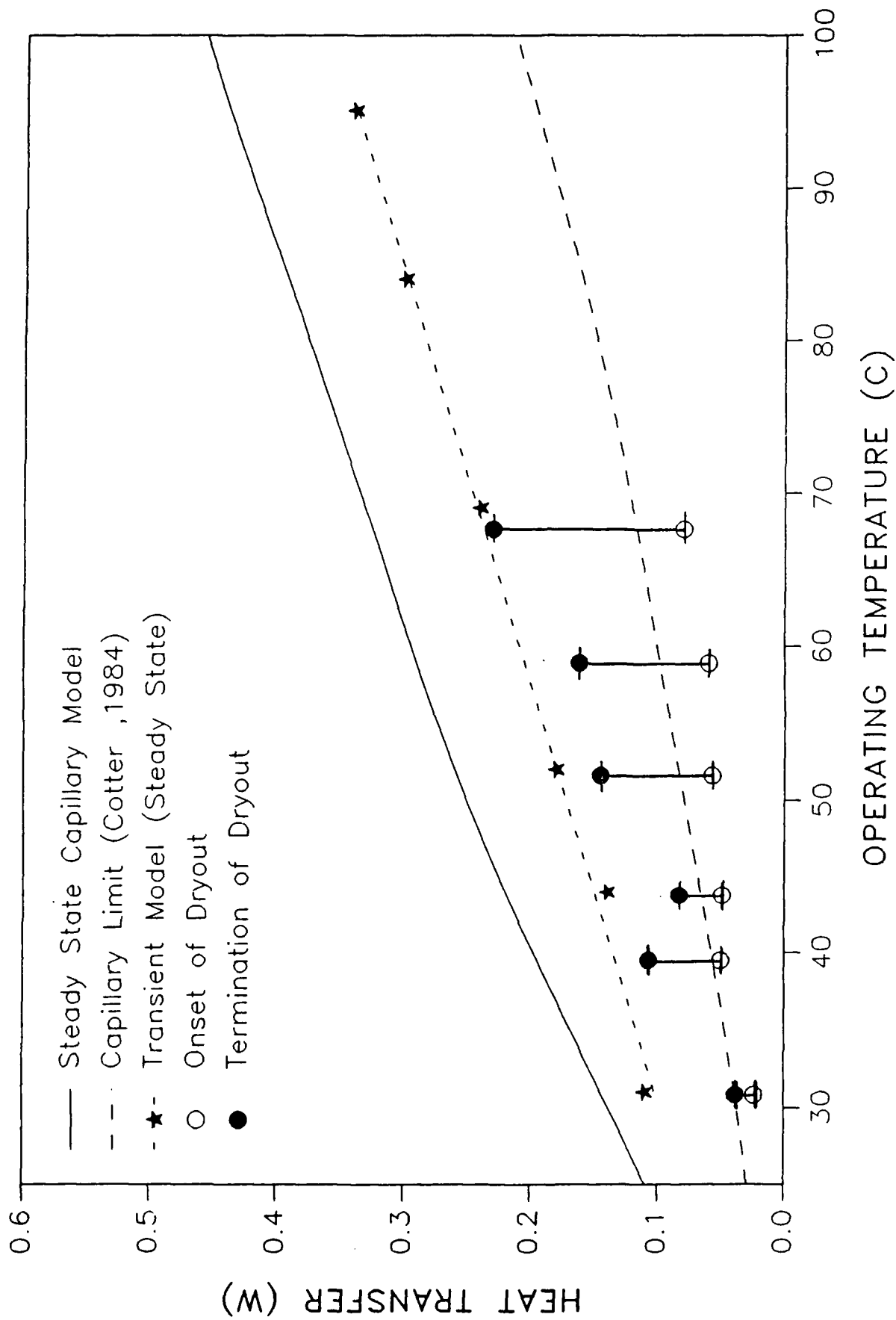


Fig. 22 Comparison of the maximum heat transport capacity of a trapezoidal micro heat pipe as a function of the operating temperature (copper, 0.0032 gm charge).

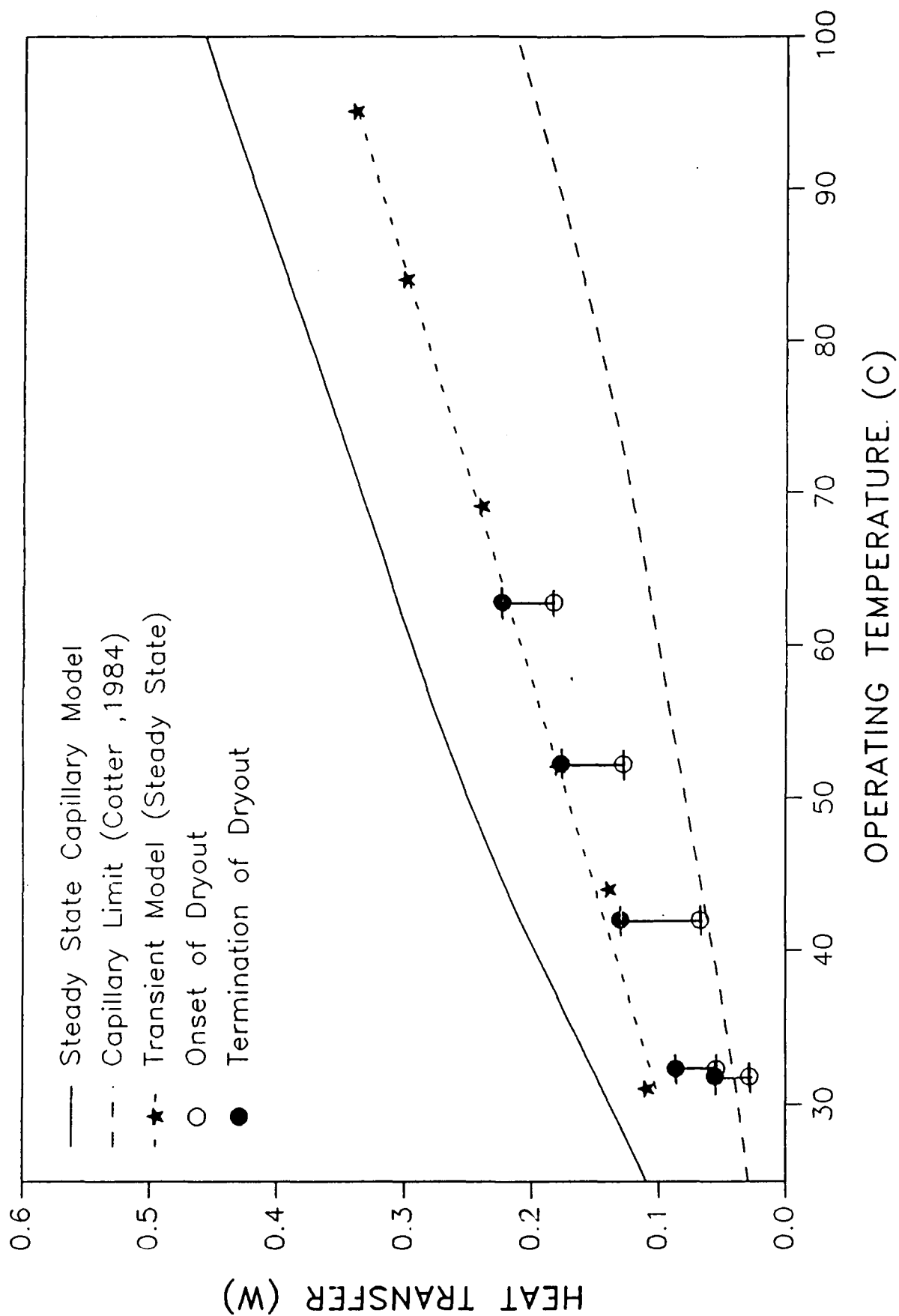


Fig. 23 Comparison of the maximum heat transport capacity of a trapezoidal micro heat pipe as a function of the operating temperature (silver, 0.0032 gm charge).

although no rationale can be made for using 0.5 as opposed to 1.00 or 0.25, which would significantly under and overestimate the values respectively.

In addition to accurately predicting the maximum heat transport capacity, the results indicated that reverse liquid flow occurs in the liquid channels during start-up and that the wetting angle is the single most important factor contributing to the transport capacity and behavior of these micro heat pipes.

5.2 Summary

The results of the modeling effort indicated that unlike traditional heat pipes, reverse liquid flow occurs in the liquid channels of the trapezoidal micro heat pipes studied here during start-up, and that the wetting angle is the single most important factor contributing to the transport capacity and behavior of these types of heat pipes.

The steady-state experimental results verified the operation of the trapezoidal micro heat pipe and when compared with the analytical model verified the trends predicted by both the steady-state model and the transient model (at steady-state). Although additional work is required to refine the models, either the steady-state or the transient model (at steady-state) could be used to accurately assess the effects of variations in the physical geometry, the amount or type of working fluid, and the power levels, all at steady-state. The Cotter model (Cotter, 1984) is of limited value unless the value for the parameter $H(L)$ is known in advance.

Since variations in the way dryout is defined can significantly increase or decrease the measured values, the discrepancy between the experimentally measured values and the predicted values may in part be due to the technique used to define dryout. As a result, the perceived accuracy of the models is strongly dependent upon how dryout is defined. To resolve this problem, it is necessary to better understand the dryout phenomena and better define when it

begins and how it proceeds.

Although the two analytical models developed have been shown to predict the steady-state performance limitations and operational characteristics with a reasonable degree of accuracy, no experimental data on the transient operational characteristics were obtained. In addition, several factors which significantly affect both the steady-state and transient behavior require continued study.

First among these is a determination of the effect of variations in the cross-sectional shape of the device; second is the effect of variations in the amount of working fluid; and third, is a determination of just how small these devices can be and still continue to function.

We recommend that both the experimental and analytical investigations be continued, to address these and other issues. The following tasks provide a logical continuation of the present effort:

- i. Using the transient model, the effect of variations in the cross-sectional shape of the device should be investigated. The present shape should be analyzed to determine how accurately it matches the shape as specified by the manufacturer. In addition, the cross-sectional shape should be optimized with respect to maximizing the heat transport capacity and the combined effect of the wetting angle and the shape determined. Shapes other than the present trapezoidal cross-section should also be investigated, including triangular and irregular polygons.
- ii. Again using the transient model, the effect of variations in the amount of working fluid should be studied. The results of this investigation indicate that since the liquid-vapor interface changes continually along the pipe, and hence, micro heat pipes are very sensitive to the amount and type of working fluid present. In addition, the wetting angle has been identified as one of the critical parameters in the determination of the maximum heat transport capacity. For these reasons, determination of the effects of both over and under filling on the transport characteristics, along with the development of a method by which the amount of fluid charge can be optimized is critical to the successful application of these devices.
- iii. One of the most significant applications of micro heat pipes is the incorporation of these devices into silicon or gallium arsenide semiconductor chips as described previously. In order to accomplish this, information is required to determine how continued reductions in the size of these devices affects their performance. This could be done using the previously developed analytical model.

- iv. To incorporate micro heat pipe technology into the applications mentioned previously, we should understand their transient behavior. The transient model has been shown to accurately predict the steady-state behavior of micro heat pipes, but the predicted transient behavior has not as yet been analyzed or compared with the results of experimental tests. Therefore, the experimental investigation should be continued to measure the transient characteristics of the test pipes. Because of the small characteristic dimensions of the test articles, the thermal measurements would need to be made using an infrared camera. Upon completion of the experimental tests, the results should be compared with the transient model to determine how accurately the transient behavior effects can be predicted. Once verified, the transient behavior of the optimized heat pipe could be evaluated.

VI. NOMENCLATURE

A	Cross-section area
a	Included angle of the groove
B	Correction factor (constant)
C	Constant
C _p	Specific heat
d	Dimension, diameter
f	Friction
g	Gravity
j	Evaporation
K ₁	permeability
K ¹	Shape factor
L	Latent heat, length
m	Mass flowrate
M	Molecular weight
P	Pressure
Q	Heat transfer weight
R	Universal gas constant
r	Radius of curvature
Re	Reynold's number
r _h	Hydraulic radius
T ^h	Temperature
V	Velocity
Vol	Volume
w	Groove width, vapor velocity
w _p	Wetted perimeter
W	Gas velocity
We	Weber number

Greek Alphabet:

α	Half included angle
β	Dimensionless variable
δ	Specific heat ratio
ϵ	Wick porosity
θ	Contact Angle
μ	Viscosity
ρ	Density
σ	Liquid surface tension
τ	Shear stress
ω	Groove width
\dagger	Tilt angle

Subscripts:

a	Adiabatic
b	Boundary, boiling
c	Capillary
d	Diagonal
e	Evaporator, entrainment
ec	Evaporation-condensation
eff	Effective
f	Friction

g	Groove
h	Hydraulic
i	Inner
in	Input
l	Liquid
m	Momentum, mean
n	Nucleation
o	Outer
out	Output
p	Pipe
s	Solid
v	Vapor, viscous
	Parallel

REFERENCES

Chi, S. W., 1976, Heat Pipe Theory and Practice, McGraw-Hill Publishing Company, New York.

Colwell, G. T. and Chang, W. S., 1984, "Measurements of the Transient Behavior of a Capillary Structure Under Heavy Thermal Loading," Int'l J. of Heat and Mass Transfer, Vol. 27, No. 4, pp. 541-551.

Cotter, T. P., 1984, "Principles and Prospects of Micro Heat Pipes," Proc. 5th Int'l. Heat Pipe Conf., Tsukuba, Japan, pp. 328-335.

Dunn, P. D. and Reay, D. A., 1982, Heat Pipes, 3rd edition, Pergamon Press, New York.

Kraus, A. D. and Bar-Cohen, A., 1983, Thermal Analysis and Control of Electronic Equipment, McGraw Hill Publishing Company, New York.

Rice, G. and Fulford, D., 1987, "Influence of a Fine Mesh Screen on Entrainment in Heat Pipes," Proc. 6th Int'l. Heat Pipe Conf., Grenoble, France, 168-172.